博士論文

Multidimensional analyses of *Cyclin-dependent kinase-like 5 (CDKL5)*, a causative gene for neurodevelopmental disorders

(神経発達障害の原因遺伝子 *Cyclin-dependent kinase-like 5 (CDKL5)* の多元的解析)

奥田　耕助

Contents

Abstract

Mutations in the *Cyclin-dependent kinase-like 5 (CDKL5)* gene cause severe neurodevelopmental disorders associated with intractable epilepsies, i.e. X-linked West syndrome or atypical Rett syndrome. Severity and heterogeneity of these disorders suggests critical roles of CDKL5 in neural development and functions. In order to elucidate the *in vivo* pathomechanisms caused by *CDKL5* mutations and the molecular functions of CDKL5, I have analyzed the phenotypes of *Cdkl5* KO mice which were generated in our laboratory. *Cdkl5* KO mice were vital and fertile. Body weight, brain weight, and gross anatomy of the brain of *Cdkl5* KO mice were not altered. However, the *Cdkl5* KO mice displayed altered dendritic branching and spine morphology of hippocampal pyramidal neurons. Behavioral analyses of the KO mice revealed enhanced anxiety-like behaviors, modulated depression-like behaviors, and impaired working and long-term memory. Intriguingly, *Cdkl5* KO mice showed normal sensitivity to kainic acid (KA) or pentylenetetrazol (PTZ), but displayed significantly enhanced seizure susceptibility in response to N-methyl-D-aspartate (NMDA). Biochemical analyses revealed aberrantly accumulated GluN2B at postsynapses of the *Cdkl5* KO mice, and this was associated with postsynaptic accumulation of SAP102, a MAGUK family scaffolding protein preferentially associated with GluN2B. These data suggest that CDKL5 regulates synaptic targeting of GluN2B via SAP102 clustering, and that loss-of-function of the CDKL5 leads to impaired learning and memory, emotion, and higher seizure susceptibility via aberrant NMDA receptor-mediated synaptic transmission.

1. Introduction

1.1 *Cyclin-dependent kinase-like 5 (CDKL5)* gene

The *Cyclin-dependent kinase-like 5 (CDKL5)* gene (OMIM #300203) was positionally cloned as a putative kinase gene named *Serine-Threonine Kinase 9 (STK9)* in 1998, through the transcriptional mapping project on Xp22 (Xp22.3-p21.3) region, where a number of human genetic disorders had been mapped including keratosis follicularis spinulosa decalvans (KFSD), Nance-Horan (NH) syndrome, X-linked dominant cone-rod degeneration (RP15), oral-facial-digital syndrome type 1 (OFD1), craniofrontonasal syndrome (CFNS), and nonsyndromic sensorineural deafness (DFN6) (Montini et al., 1998). Based on its sequence homology to the *Cyclin-dependent kinase (CDK)* family, the *STK9* gene was renamed as *Cyclin-dependent kinase-like 5 (CDKL5)*, a member of the *Cyclin-dependent kinase-like (CDKL)* family by the HUGO Gene Nomenclature Committee (HGNC). CDKL family consists of five members, i.e. CDKL1 - CDKL5, and belongs to the CMGC (CDK, MAPK, GSK3, CLK) group in the human kinome (Manning et al., 2002).

Human *CDKL5* gene is located in Xp22, spanning 228kb, containing 24 exons (exons 1, 1a, 1b, 2 - 16, 16b, 17 - 21) (Kalscheuer et al., 2003; Kilstrup-Nielsen et al., 2012)(Fichou et al., 2011). Translation starts in exon 2, and terminates in intron 18 (mRNA: 3136 bp, protein: 960 amino acids, 107 kDa) or in exon 21 (mRNA: 3434bp,: protein: 1030 amino acids, 115 kDa) by alternative splicing (Fig. 1). The 107 kDa isoform is the predominant transcript in brain, and the 115 kDa isoform is expressed specifically in testis (Williamson et al., 2012). An additional splice variant containing exon 16b (123 bp, 41 amino acids), located between exons 16 and 17, is expressed specifically in brain (Fichou et al., 2011).

1.2 Mutations in the *CDKL5* gene

In 2003, mutations in the *CDKL5* gene were identified in the patients with severe X-linked infantile spasms and mental retardation (Kalscheuer et al., 2003). Since then, more than 100 cases with *CDKL5* mutations have been reported (Bahi-Buisson and Bienvenu, 2012). Majority of diagnosed patients were female, however recent reports have seen fair number of hemizygous male patients (Elia et al., 2008; Liang et al., 2011). Accurate sex ratio as well as sex difference in phenotypic severity of *CDKL5*-related disorders are not established yet.

Clinical characteristics associated with *CDKL5* mutations are: (i) normal prenatal history; (ii) irritability, drowsiness and poor sucking in the perinatal period before seizure onset; (iii) early-onset epilepsy usually before 5 months of age; (iv) Rett-like features consisting of deceleration of head growth, stereotypies, poor to absent voluntary hand use, and sleep disturbances, and (v) severe mental retardation with poor eye contact and virtually no language (Bahi-Buisson and Bienvenu, 2012; Bahi-Buisson et al., 2008b; Hagberg and Skjeldal, 1994; Nemos et al., 2009; Neul et al., 2010). The core symptom of *CDKL5*-related disorders is described as epileptic encephalopathy often associated with Rett-like features. Clinical manifestations change according to the growth and development of the patients. Bahi-Buisson *et al.*, demonstrated that *CDKL5*-related epileptic encephalopathy is characterized by a 3-stage evolution: (stage 1: onset 1–10 weeks) early epilepsy with normal interictal electroencephalogram (EEG) despite frequent convulsive seizures; (stage 2: 6 months - 3 years) epileptic encephalopathy with infantile spasms and hypsarrhythmia; (stage 3: 2 ½ years-) refractory epilepsy with tonic seizures and myoclonia (Bahi-Buisson et al., 2008a).

Accordingly these patients have been diagnosed either as, early infantile epileptic encephalopathy-2 (EIEE2) (OMIM #300672), X-linked West syndrome, or atypical Rett syndrome Hanefeld variant.

CDKL5 mutations cause disease phenotypes in an X-linked dominant fashion. Mutations are *de novo* in all reported cases, and include point mutations, deletions as well as duplications. Until 2012, 23 missense, 10 nonsense, 25 frameshift, and 14 splice mutations have been described as point mutations (Bahi-Buisson and Bienvenu, 2012) (Fig. 2). The most prominent feature of the *CDKL5* mutations is that all missense mutations except one cluster within exon 2-11 corresponding to the N-terminal kinase domain, and other mutations are distributed randomly throughout the gene (Fig. 2). The recombinant protein experiments have shown that missense mutations within the kinase domain impair the kinase activity of the CDKL5 protein (Bertani et al., 2006). Interestingly, duplications of the X-chromosomal region containing *CDKL5* gene were identified in patients with X-linked mental retardation (Froyen et al., 2007; Tzschach et al., 2008).

Phenotypes associated with *CDKL5* mutations have variation ranging from milder forms to severe forms. So far no clear genotype-phenotype correlation of mutations has been established (Bahi-Buisson and Bienvenu, 2012; Kilstrup-Nielsen et al., 2012).

1.3 Molecular functions of the CDKL5 protein

The CDKL5 protein is a serine/threonine kinase sharing homology to CDKs and MAPKs (Fig. 3). The kinase domain lies at the N-terminus corresponding to exons 2-11 (Fig. 2). Similar to MAPKs, CDKL5 autophosphorylates the TEY (Thr-Glu-Tyr) motif in the kinase domain (Bertani et al., 2006). Unlike MAPKs or CDKs, CDKL5

has a long C-terminal region spanning 700 amino acid length (Fig. 3). In rodents, CDKL5 protein is widely distributed in all tissues, with highest levels in brain, thymus, and testis (Lin et al., 2005). In mouse, the expression starts as early as E7.5, strongly increases in early postnatal stage, then declines slowly up to adult stage, and persists throughout life (Lin et al., 2005; Rusconi et al., 2008). CDKL5 protein is localized in the neuronal nucleus and cytoplasm, and its subcellular distribution is regulated by the C-terminal region and the kinase activity (Bertani et al., 2006; Lin et al., 2005; Rusconi et al., 2008).

Based on the subcellular localization profile, CDKL5 is believed to play multiple roles in neurons. Mari *et al.* reported that CDKL5 phosphorylated the protein complex of MECP2 (methyl CpG binding protein 2), a Rett-syndrome causing gene product, suggesting a functional crosstalk with MECP2 pathway (Mari et al., 2005). Ricciardi *et al.* showed that CDKL5 localized to nuclear speckles in cells and controlled their morphology, which was dependent on its kinase activity. They further showed that CDKL5 influenced alternative splicing in heterologous minigene assays. These data suggest that CDKL5 is involved in pre-mRNA processing by controlling splicing factor dynamics (Ricciardi et al., 2009).

In the cytoplasm, CDKL5 has been shown to be localized in neurites, growth cones, dendrites, and dendritic spines (Chen et al., 2010; Ricciardi et al., 2012; Rusconi et al., 2008). Chen *et al.* demonstrated that knockdown of CDKL5 inhibited neurite growth and dendrite arborization, whereas overexpression had opposite effects. They showed that in fibroblasts and neurons, CDKL5 colocalized and formed a protein complex with Rac1, and overexpression of Rac1 prevented the knockdown effects of CDKL5, suggesting that Rac1 acts downstream of CDKL5 in neuronal morphogenesis.

They further showed that CDKL5 was required for brain-derived neurotrophic factor (BDNF)-induced activation of Rac1 (Chen et al., 2010). Ricciardi *et al.* showed that CDKL5 was localized at excitatory synapses and phosphorylated the cell adhesion molecule NGL-1. This phosphorylation ensured a stable association between NGL-1 and PSD95. CDKL5 knockdown altered spine morphology and synaptic activity. Phospho-mimicking form of NGL-1 was bound to PSD95 more efficiently and partially rescued the CDKL5-specific spine defects (Ricciardi et al., 2012). Zhu *et al.* reported that CDKL5 interacted with palmitoylated PSD-95, and its interaction regulated synaptic targeting of CDKL5 (Zhu et al., 2013).

In December 2012, Wang *et al.* reported the development of the *Cdkl5* knockout (KO) mouse and showed its autistic-like deficits in social interaction, as well as impairments in motor control and fear memory, and alterations in event-related potentials (ERPs). The *Cdkl5* KO mouse kinome profiling revealed disruption of multiple signal transduction pathways, including the AKT-mammalian target of rapamycin (mTOR) cascade (Wang et al., 2012).

1.4 Aims of my research

As described above, the loss of CDKL5 leads to severe neurological disorders, but our understanding of its pathophysiological mechanisms and its molecular functions is scarce and fragmented. *In vivo* investigation is necessary to elucidate these. The aims of my research is to disclose the *in vivo* pathomechanisms caused by the loss of CDKL5 and the molecular functions of CDKL5 by investigation into the *Cdkl5* KO mice.

2. Materials and methods

All animal experiments and recombinant DNA experiments in this research were approved by the institutional review committees of the Graduate School of Medicine, The University of Tokyo and National Institute for Physiological Sciences.

Cdkl5 knockout mouse

The *Cdkl5* KO mouse line was generated by the former graduate student, Ms. Aya Watanabe, and Associate Professor Teruyuki Tanaka as follows. The mouse *Cdkl5* gene consists of 19 exons spanning 210,373 bp of genomic DNA on chromosome X. The translation initiation site lies within exon 2, and the serine-threonine kinase domain corresponds to exons 2 – 11. In order to generate the *Cdkl5* flox mouse, the exon 2 was targeted by flanking two loxP sites (Fig. 4A). The linearized targeting vector was electroporated into the mouse TT2F ES cells, and homologous recombination was detected in 15 clones. After blastocyst injection of one clone and subsequent transplantation in a surrogate mother, chimeric mice with germline transmission were obtained. *Cdkl5* flox/+ heterozygous and *Cdkl5* flox/Y hemizygous mice were successfully generated by crossing the germline chimeras with C57BL/6N wild type mice (Fig. 4A). By crossing the *Cdkl5* flox/Y hemizygous male mouse with CAG-*cre* transgenic female mouse, which mediate the site-specific recombination of paternally derived target gene upon fertilization, *Cdkl5* heterozygous and hemizygous knockout mice were successfully obtained (Fig. 4B) (Sakai and Miyazaki, 1997). By crossing the *Cdkl5* +/- female with wild-type male, *Cdkl5* +/+ female, +/- female, +/Y male, and -/Y male mice were generated. In this research, I used *Cdkl5* +/Y male mice designated as wild-type (WT) mice, and *Cdkl5* -/Y male mice designated as *Cdkl5* KO mice. Western blotting of the brain lysates from *Cdkl5* -/Y and -/+ mice showed

complete loss and 50% reduction of CDKL5 immunoreactivity respectively, thus confirming the successful targeting of the *Cdkl5* gene in the knockout mouse line (Fig. 4C). The *Cdkl5* flox/Y hemizygous male mouse showed decreased level of CDKL5 immunoreactivity (Fig. 4C). This is because the *Cdkl5* floxed allele retains a large domain of PGK-Neo in its intron 3, which may interfere with the transcription of *Cdkl5* gene.

Sholl analysis

In order to image and analyze dendritic arborization and morphology of the hippocampal neurons of the *Cdkl5* KO and control mice, I have adopted Neurolucida system (MBF Bioscience, Inc. Williston, VT). Two hundred and forty μm thick coronal slices of Golgi-Cox stained brains were prepared using FD Rapid GolgiStain Kit (FD NeuroTechnologies, Inc. Columbia, MD) as manufacture's instruction. Hippocampal CA1 regions captured by Leica DM6000 B upright microscope using 40x lens were monitored on computer display and traced using the Neurolucida software. I imaged 8 – 10 neurons from each mouse, and totally measured 34 neurons from WT mice and 32 neurons from KO mice. Concentric circles (Sholl lines) were drawn at 10 μm increments up to a radius of 180 μm for basal dendrites, or 310 μm for apical dendrites from the center of the soma. Following parameters were measured: (1) the size of cell body, (2) number of dendrites, (3) number of nodes, (4) number of endings, (5) total length of dendrites, (6) each length of dendrites, (7) the number of intersection in every 10 micrometers from the center of cell body, (8) the number of nodes in every 10 micrometers from the center of cell body, (9) the number of endings in every 10 micrometers from the center of cell body. All measurements were performed

blindfolded manner as to genotypes. Parameters (1), (2), (3), (4), (5) and (6) were statistically analyzed by ANOVA, and parameters (7), (8) and (9) were statistically analyzed by repeated measure ANOVA.

Spine analyses

In order to image the spines by the laser confocal scanning microscopy, I crossed the *Cdkl5* KO mouse line with Thy1-EGFP line M transgenic mouse (Feng et al., 2000). Thy1-EGFP M line mouse expresses EGFP in sparse subset of neurons under the control of a modified Thy1 promoter, enabling clear and bright Golgi-like stain. Thy1-EGFP positive *Cdkl5* -/Y and +/Y mice were euthanized and transcardially perfused with PBS followed by 4% paraformaldehyde (PFA) in PBS. Brains were removed and drop fixed in 4% PFA for 60 min. Fifty μm thick brain slices were cut using the vibrating microslicer DTK-1000 (D.S.K). Apical dendrites of CA1 pyramidal neurons were imaged by the laser scanning confocal microscope FV1000-D (Olympus) using 60x oil lens (NA 1.35). Image acquisition was performed with 2048 x 2048 pixel size and 0.1 μm slice interval (Voxel size: 0.1 μm ^3). Secondary and tertiary branches of apical dendrites located between 100 and 180 μm from the cell body layer were selected to analyze using Imaris 7.4 software (Bitplane). The Imaris FilamentTracer with AutoDepth Method was used to trace dendrites in Surpass view. After centering filaments, "Rebuild Dendrite Diameter" was performed. Dendrite Threshold (local contrast) was automatically set. Spine seed point was set to 0.15 μm and maximum length was set to 3 μm. Spine Seed Points Threshold was automatically set and adjusted manually such that all visually discernible spines were detected. Spine Threshold (local contrast) was set at 3. After rendering, I removed

the spines which had 0 - 30 degrees of Spine Orientation Angle from the Z-axis, because the confocal microscopic images had Z-axis blurring, which might lead to errors in automatic rendering. Parameters such as dendrite length, dendrite area, dendrite number of spines, dendrite spine density, and spine length, were automatically obtained from the rendered dendrites and spines. Eight thousand one hundred and fifty spines from 29 WT neurons and 6,831 spines from 32 KO neurons were analyzed. All parameters were statistically analyzed by t-test.

For the spine type classification, the above confocal images were deconvoluted by AutoQuant X3 software (Media Cybernetics) and analyzed with NeuronStudio software (Computational Neurobiology and Imaging Center). "Spine Classifier" in the NeuronStudio was applied to classify spines into either stubby, thin, or mushroom, with the following parameters; Neck Ratio 1.100, Thin Ratio 2.500, Mushroom Size 0.350 μm. All data were statistically analyzed by student t-test.

Behavioral phenotyping

In this research, I performed all behavioral tests of *Cdkl5* KO and control mice in the Section of Behavior Patterns, Center for Genetic Analysis of Behavior, National Institute for Physiological Sciences under the instruction of Professor Tsuyoshi Miyakawa and Associate Professor Keizo Takao. There, Professor Miyakawa had established the comprehensive behavioral test battery system for mutant mice, and has obtained behavioral profiles of more than 160 strains. The test battery contains more than 20 tests to cover sensori-motor functions, emotion, attention and learning/memory (Table 1) (Takao and Miyakawa, 2009).

For the initial screening, I performed general health and neurological screening,

hot plate test, rotarod test, gait analysis, prepulse inhibition test, light/dark transition test, open field test, elevated plus maze, social interaction test, Porsalt swim test, tail suspension test, fear conditioning test and passive avoidance test. Twenty-two *Cdkl5* KO male mice and 22 control male mice of 9 to 10 weeks of age were transported from the animal facility of The University of Tokyo, School of Medicine. Those mice had been backcrossed with C57BL/6N by 6 generations. After 1 week habituation, I started behavioral testing. For the assessment of learning and memory functions of the KO mice, I transported other 22 *Cdkl5* KO male mice and 22 control male mice of 9 to 10 weeks of age (backcrossed with C57BL/6N by 8 generations). After habituation, I performed Barnes maze test, Y-maze test and T-maze test as the learning/memory tests.

General health and neurological screening

General health and neurological screen examines body weight, rectal temperature, whisker, coat, simple reflexes and muscle strength. Grip strength test and wire hang test were used to measure muscle strength. Grip strength was measured by using a grip strength meter (O'Hara & Co., Tokyo, Japan) as previously reported (Matsuo et al., 2010). Each mouse was lifted by its tail, and grasped a wire grid by its forepaws. Then, the mouse was gently pulled back by the tail. The peak force applied by forelimbs of the mouse was recorded. In the wire hang test, latency to fall from an inverted wire mesh was recorded. Data were statistically analyzed by ANOVA.

Hot Plate test

A pain sensitivity was measured by the hot plate test according to previous report (Matsuo et al., 2010). Each Mouse was placed on a 55 ^{o}C hot plate (Columbus

Instruments), and latency to the first hindpaw lick was recorded. Data was statistically analyzed by ANOVA.

Rotarod test

Motor coordination and motor learning was assessed by the rotarod test (Matsuo et al., 2010). Each mouse was placed on a rotating drum with 3 cm diameter (UGO Basile Accelerating Rotarod), and latency to fall from the rotarod was recorded. The speed of the rotarod accelerated from 4 to 40 r.p.m over a 5-min period. This test was performed three times per day, and total six trials were performed in two days. Data was statistically analyzed by repeated measure ANOVA.

Gait analysis

The gait of the *Cdkl5* KO and control mice during spontaneous walk/trot locomotion on a translucent plate was shot by a high speed camera (150 flame/sec.) from underneath. Footprint patterns were analyzed on distance between each stride, variability in stride length, variability around a liner axis, stance width of frontpaws and hindpaws (Crawley, 2007; Yao et al., 2011). All Data were statistically analyzed by ANOVA.

Startle response / Prepulse inhibition test

For the assessment of sensorimotor gating, a startle reflex measurement system (O'Hara & Co., Tokyo, Japan) was used to measure startle response and prepulse inhibition as previously described (Matsuo et al., 2010). A mouse was placed in a plastic cylinder and left undisturbed for 10 min for acclimatization. White noise (40

ms) was used as the stimulus. The intensity of the startle stimulus was 110 or 120 dB, and the prepulse stimulus was presented 100 ms before the startle stimulus, and its intensity was 74 or 78 dB. The startle response was recorded for 140 ms starting with the onset of the prepulse stimulus. A test session consisted of six trial types (i.e., two types for startle stimulus only trials, and four types for prepulse inhibition trials). Four combinations of prepulse and startle stimuli were used (74–110, 78–110, 74–120, and 78–120 dB). Six blocks of the six trial types were presented in pseudorandom order such that each trial type was presented once within a block. The average inter-trial interval was 15 s (range 10–20 s). All data were statistically analyzed by ANOVA.

Light/dark transition test

A light/dark transition test was performed as previously described (Takao and Miyakawa, 2006). The apparatus consisted of a cage (21 x 42 x 25 cm) divided into two sections of equal size by a partition with a door (Ohara & Co., Tokyo). One chamber was brightly lit (390 lux), whereas the other chamber was dark (2 lux). A mouse was placed into the dark side and allowed to move freely between the two chambers with the door open for 10 min. The total number of transitions, latency to first enter the light chamber, distance traveled, and time spent in each chamber were recorded. All data were statistically analyzed by ANOVA.

Open field test

Open field test was performed as previously described (Takao et al., 2010). Each mouse was placed in the corner of the VersaMax open field apparatus (40 x 40 x 30 cm; AccuScan Instruments, Columbus, OH). The chamber of the test was lit at 100

lux. Total distance traveled, vertical activity (rearing measured by counting the number of photobeam interruptions), time spent in the center area (20 x 20 cm), and beam-break counts for stereotyped behaviors were recorded for 120 min. All data were statistically analyzed by repeated measure ANOVA.

Elevated plus maze

Elevated plus maze test was performed as previously described (Komada et al., 2008; Takao et al., 2010). The apparatus consisted of two open arms (25 x 5 cm) and two enclosed arms of the same size with 15 cm high transparent walls. The arms and central square were made of white plastic plates and were elevated 55 cm above the floor. 0.3 mm high Plexiglas walls surrounded the sides of the open arms to minimize the likelihood of mice falling. Arms of the same type were oriented opposite from each other. Each mouse was placed in the central square of the maze (5 x 5 cm), facing one of the closed arms. Mouse behavior was recorded for 10 min. The number of entries into open arms, and the time spent in the open and enclosed arms were recorded. Percentage of entries into open arms, time spent in open arms, number of total entries, and total distance traveled were analyzed. Data acquisition and analysis were performed automatically. All data were statistically analyzed by ANOVA.

Porsolt forced swim test

Porsolt swim test was performed as previously described (Matsuo et al., 2010; Takao et al., 2010). The apparatus consisted of four Plexiglas cylinders (20 cm height x 10 cm diameter). The cylinders were filled with water (23 ^{O}C), up to a height of 7.5

cm. Mice were placed in the cylinders, and the immobility and the distance traveled were recorded for 10 min. Images were captured at one frame per second.

For each pair of successive frames, the amount of area (pixels) within which the mouse moved was measured. When the amount of area was below a certain threshold, mouse behavior was judged as "immobile." When the amount of area equaled or exceeded the threshold, the mouse was considered as "moving." Data acquisition and analysis were performed automatically. All data were statistically analyzed by repeated measure ANOVA.

Tail suspension test

Tail suspension test was performed as previously described (Takao et al., 2010). Mice were suspended 30cm above the floor by adhesive tape placed 1cm from the tip of the tail, and the immobility was recorded for 10 min. Data acquisition and analysis were performed automatically. Data was statistically analyzed by repeated measure ANOVA.

Social interaction test in a novel environment (one chamber social interaction test)

Social interaction test in a novel environment was performed as previously described (Tanda et al., 2009). Two mice of the same genotypes that were previously housed in different cages were placed in a 40 × 40 × 30 cm box together and allowed to explore freely for 10 min. Mouse behaviors were recorded with a CCD camera.

The total number of contacts, total duration of active contacts, total contact duration, mean duration per contact, and total distance traveled were measured automatically.

The active contact was defined as follows. Images were captured at 1 frame per

second, and distance traveled between two successive frames was calculated for each mouse. If the two mice contacted each other and the distance traveled by either mouse was longer than 2 cm, the behavior was considered as 'active contact'. All data were statistically analyzed by ANOVA.

Crawley's Sociability and Social Novelty Preference Test (three chamber social interaction test)

In addition to Social interaction test in a novel environment (one chamber social interaction test), Crawley's Sociability and Social Novelty Preference Tests were conducted in order to evaluate social behaviors from various angles. Tests were performed as previously described (Miyakawa et al., 2001; Takao et al., 2010). The testing apparatus consisted of a rectangular, three-chambered box and a lid with an infrared video camera (Ohara & Co., Tokyo). Each chamber was 20 cm x 40 cm x 22 cm and the dividing walls were made of clear Plexiglas, with small square openings (5 cm x 3 cm) allowing access into each chamber. An unfamiliar C57BL/6 male (stranger 1), that had had no prior contact with the subject mouse, was placed in one of the side chambers. The location of stranger 1 in the left vs. right side chamber was systematically alternated between trials. The stranger mouse was enclosed in a small, round wire cage, which allowed nose contact between the bars, but prevented fighting. The cage was 11 cm in height, with a bottom diameter of 9 cm, vertical bars 0.5 cm, and horizontal bars spaced 1 cm apart. The subject mouse was first placed in the middle chamber and allowed to explore the entire social test box for a 10-min session. The amount of time spent in each chamber and number of entries into each chamber was measured. Each mouse was tested in a 10-min session to quantify social preference for

the first stranger. After the first 10-min session, a second unfamiliar mouse was placed in the chamber that had been empty during the first 10-min session. This second stranger was also enclosed in an identical small wire cage. The test mouse thus had a choice between the first, already-investigated unfamiliar mouse (stranger 1), and the novel unfamiliar mouse (stranger 2). The amount of time spent in each cage during the second 10-min and number of entries into each cage was measured as described above.

Total distance and average speed were statistically analyzed by ANOVA between genotypes. Other measurements were statistically analyzed by ANOVA between each cage within genotypes.

24-hour Monitoring in Home Cage

Twenty-four hour monitoring in the home cage was conducted as previously described (Miyakawa et al., 2003; Takao et al., 2010). Two mice of the same genotype that had been housed separately were placed together in a home cage (29 x 18 x 12 cm) attached with an infrared video camera. Their social behaviors and locomotor activities were then monitored for 1 week. Images from each cage were captured at a rate of 1 frame per second. Social interaction was measured by counting the number of particles detected in each frame: two particles indicated that the mice were not in contact with each other; and one particle indicated contact between the two mice. Locomotor activity was measured by quantifying the number of pixels that changed between each pair of successive frames. Data acquisition was performed automatically. All data were statistically analyzed by repeated measure ANOVA within total time, day time and night time.

Contextual and cued fear conditioning

Fear conditioning tests were performed as previously described (Takao et al., 2010). Each mouse was placed in a cuboid chamber (26 x 34 x 29 cm) and allowed to explore freely for 2 min. A 60 dB white noise, which served as the conditioned stimulus (CS), was presented for 30 secs, followed by a mild (2 secs, 0.5 mA) footshock, which served as the unconditioned stimulus (US). Two more CS-US pairings were presented with a 2-min inter-stimulus interval. Context testing was conducted 24 h, 7 days after conditioning in the same chamber. Cued testing with altered context was conducted after conditioning using a triangular chamber (35 x 35 x 40 cm) made of white opaque Plexiglas. Images were captured at 1 frame per second. For each pair of successive frames, the amount of area (pixels) by which the mouse moved was measured. When this area was below a certain threshold, the behavior was judged as 'freezing'. When the amount of area equaled or exceeded the threshold, the behavior was considered as 'non-freezing'. Data acquisition, control of stimuli (i.e. tones and shocks), and data analysis were performed automatically. All data were statistically analyzed by repeated measure ANOVA. In the cued test with altered context, all data were separately analyzed in pre-tone duration and tone duration.

Passive avoidance test

Passive avoidance test was performed as previously described (Takao et al., 2010). The apparatus consisted of one dark and one bright chamber connected by a sliding door (Ohara & Co., Tokyo). Each mouse was first placed into the bright chamber and the door was opened. After a mouse entered the dark chamber, a 2-sec footshock at 0.3 mA was delivered to the mouse. Mice that did not enter the dark

chamber within 600 sec were scored as 600 sec. One the day 1, day 2, and day 8, animals were tested for retention by placing each animal into the bright chamber and the latency of the mouse entering the dark chamber was statistically analyzed by ANOVA.

Barnes maze test

Barnes maze was performed as previously described (Harrison et al., 2006; Takao et al., 2010). The Barnes maze apparatus consisted of a white circular disk 1.0 m in diameter with 12 holes equally spaced around the perimeter (Ohara & Co., Tokyo). The disk was elevated 75 cm from the floor. A black escape box (17 x 13 x 7 cm), which had paper cage bedding on its bottom, was located under one of the holes, which represented the target. The location of the target was consistent for a given mouse but randomized across mice. The maze was rotated daily, with the spatial location of the target unchanged with respect to the distal visual room cues, to prevent a bias based on olfactory or the proximal cues within the maze. Two to three trials per day were conducted everyday until the total number of trials reached 12. The next day, a probe trial without the escape box was conducted to confirm that this spatial task was acquired based on navigation by distal environment room cues. However, the *Cdkl5* KO mice could not memorize the target hole, so further 8 trials were given to both genotypes until the KO mice were able to remember the target hole. After 1 month, probe trial tests were conducted to evaluate memory retention. Time spent around each hole was recorded by the software. Mice which had fallen from maze were excluded in the probe test. Data in training phase was statistically analyzed by repeated measure ANOVA, and data in probe test was analyzed by t-test.

T-maze test

Forced alternation task using the T-maze were performed as previously described with modifications (Shoji et al., 2012; Takao et al., 2008). The apparatus was constructed of white plastics runways with walls 25-cm high (O'Hara & Co., Tokyo, Japan). The maze was partitioned off into 6 areas by sliding doors. The stem of T was composed of area S2 (13 × 24 cm) and the arms of T were composed of area A1 and A2 (11.5 × 20.5 cm). Area P1 and P2 were the connecting passage way from the arm (area A1 or A2) to the start compartment (area S1) (Fig. 23A). Each trial consisted of one forced run followed by one free run. First the mouse was placed in S2 and forced to proceed in one direction (S2 → A2 → P2 → S1, or S2 → A1 → P1 → S1) by opening the doors successively. After returning to S2, both a1 and a2 doors were made open and the mouse was allowed to choose either direction freely. If the mouse choose the opposite direction from the previous forced run, it was counted as a correct response, and if the mouse choose the same direction as the previous run, it was counted as an incorrect response. Each mouse was given 10 trials per day, for 3 consecutive days. Data acquisition and control of sliding doors were performed automatically, and data was analyzed by two-way repeated measures ANOVA.

Drug-induced seizure susceptibility test

Seizures were induced to post-weaned (4 weeks of age) or adult (13-15 weeks of age) mice by intraperitoneal administration of either kainic acid (KA) (K0250, Sigma-Aldrich) 20 and 25 mg/kg, pentylenetetrazol (PTZ) (P6500, Sigma-Aldrich) 35 mg/kg, or N-Methyl-D-aspartic acid (NMDA) (M3262, Sigma-Aldrich) 50 mg/kg in PBS. PTZ-induced seizure grades were scored according to Westmark *et al.* as

follows: 0. No change in behavior; 1. progressive decrease in motor activity until the mouse comes to rest in a crouched or prone position with abdomen in full contact with the bottom of the cage; 2. twitches; 3. fully developed minimal seizures with clonus of the head muscles and forelimbs, with the righting reflex present; 4. major seizures involving a fall and exhibiting forelimbs that are parallel to the body axis and stiff; 5. major seizure with hyperactive bouncing followed by a fall and clonus of all four limbs (Westmark et al., 2008). KA and NMDA induced seizure grades were scored according to Wu *et al.* as follows: 0. no abnormality; 1. exploring, sniffing, and grooming ceased, becoming motionless; 2. forelimb and/or tail extension, appearance of rigid posture; 3. myoclonic jerks of the head and neck, with brief twitching movement, or repetitive movements with head bobbing or "wet-dog shakes"; 4. forelimb clonus and partial rearing, or rearing and falling; 5. forelimb clonus, continuous rearing and falling; 6. tonic-clonic movements with loss of posture tone (Wu et al., 2005). After drug injection, the max seizure scores in 60 min (PTZ and NMDA) or 120 min (KA) observation period were recorded and statistically analyzed with Mann-Whitney U test.

Subcellular fractionation

Subcellular fractionation of brain tissues was performed as described by Shin *et al.* with minor modifications (Shin et al., 2013). The cerebrum, prefrontal cortex (PFC), and hippocampus of the wild-type and *Cdkl5* KO mice were homogenized using a Potter homogenizer with 15 strokes at 1,000 r.p.m in 10 volumes of homogenization buffer (0.32 M sucrose, 4 mM HEPES pH 7.4, 1x Halt Protease Inhibitor Cocktail (Thermo Scientific)) on ice. The homogenate was centrifuged at 1,000X g for 10 min to remove the nuclear fraction (P1). The supernatant (S1) was centrifuged at 10,000 X

g for 15 min to yield the crude synaptosomal fraction (P2). The pellet was resuspended in 10 volumes of HEPES-buffered sucrose and then centrifuged at 10,000 X g for another 15 min. The resulting pellet (P2') was resuspended in 10 volume of 4 mM HEPES (pH 7.4) and lysed hypo-osmotically by homogenization with 3 strokes at max speed followed by constant mixing for 30 min at 4^{O}C. The lysate was centrifuged at 25,000 x g for 20 min at 4^{O}C and the resulting pellet (LP1) was resuspended in the homogenization buffer. LP1 fraction was layered on top of a discontinuous sucrose gradient consisting of 0.8 M, 1.0 M and 1.2 M sucrose, and centrifuged at 150,000 X g for 120 min at 2^{O}C. Synaptic plasma membranes were recovered from the 1.0/1.2 M interface and resuspended in 2.5 volumes of 4 mM HEPES. This fraction was centrifuged at 150,000 X g for 30 min at 4 ^{O}C and the resulting pellet was resuspended in 50 mM HEPES and 2 mM EDTA (pH 7.4). PSD purification was performed by adding Triton X-100 to the final concentration of 0.5%, incubation on ice for 15 min, and centrifugation at 32,000 X g for 20 min at 4 ^{O}C. The resulting pellet was resuspended in 1% SDS, 40 mM Tris-HCl pH7.5, 1x Halt Protease Inhibitor Cocktail (Thermo Scientific) to yield the PSD-1T fraction.

Western blotting

Each protein sample was combined with 5x sample buffer (60 mM 1M Tris-HCl, pH 6.8, 25% glycerol, 2% SDS, 14.4 mM 2-mercaptoethanol, 0.1% BPB) so that the sample buffer makes 1x concentration, and boiled for 5 min. Samples were separated by SDS-PAGE using the Bio-Rad Mini-PROTEAN Tetra Cell apparatus, and transferred onto the Immobilon-P Transfer Membrane (Millipore) using the Bio-Rad

Trans-Blot SD Semi-Dry Transfer apparatus. The membranes were blocked in 4% skim milk /PBS for 1 hour and incubated in primary antibodies for overnight at 4 ^{O}C. Secondary antibodies are, Anti-Rabbit IgG (whole molecule)-Peroxidase antibody produced in goat (A0545, Sigma-Aldrich) diluted at 1:1,000-5,000, or Anti-Mouse IgG (Fab specific)-Peroxidase antibody produced in goat (A2304, Sigma-Aldrich) diluted at 1:5,000. Chemi-Lumi One L (nacalai tesque) reagents were applied and chemiluminescence was detected using LAS-4000 mini (Fujifilm). Band intensity of each lane was quantitated using the Image J software (NIH). All data were statistically analyzed by t-test.

Antibodies

Following antibodies were used in this research;

anti-CDKL5 rabbit polyclonal antibody (HPA002847, Atlas antibodies),

anti-GluR1 rabbit polyclonal antibody (AB1504, Millipore),

anti-GluR2/3 rabbit polyclonal antibody (07-598, Millipore),

anti-GluN1-C2 rabbit polyclonal antibody (GluRz1-Rb-Af720, Frontier Institute),

anti-GluN2A rabbit polyclonal antibody (GluRe1C-Rb-Af542, Frontier Institute),

anti-GluN2B rabbit polyclonal antibody (GluRe2N-Rb-Af660, Frontier Institute),

anti-SAP102 rabbit polyclonal antibody (PSD102-Rb-Af218, Frontier Institute),

anti-PSD95 mouse monoclonal antibody (7E3-1B8) (ab13552, abcam),

anti- α -Tubulin mouse monoclonal antibody (T9026, Sigma-Aldrich),

anti-GST antibody produced in goat (27-4577-50, GE Healthcare).

3. Results

3.1.1 General Features of the *Cdkl5* KO mouse

Crossing *Cdkl5* +/- female with *Cdkl5* +/Y male mouse generates offspring of four genotypes (+/+, +/-, +/Y, -/Y) with expected ratio, suggesting that removal of the *Cdkl5* gene does not relate to embryonic lethality. Both *Cdkl5* +/- and -/Y mice are vital and fertile. There were no statistical differences in the body and brain weight between *Cdkl5* -/Y (KO) and +/Y (WT) mice at 5 weeks and 10 weeks of age (Fig. 5A and B). I compared Nissl-stained coronal sections of brains from *Cdkl5* -/Y and *Cdkl5* +/Y mice. No gross anatomical abnormalities were observed in the cerebral cortex, hippocampus or cerebellum (Fig. 6A-F). Comparison of KB-stained brains from two genotypes also showed similar myelination in the cerebral cortex between two genotypes (Fig. 6G and H). Previous study reported that *Mecp2* knockout mouse have smaller neuronal cells and nuclei in cerebrum, however there is no distinguishable difference in the size of neuronal cells and nuclei between *Cdkl5* -/Y and +/Y mice (Fig. 6I - N) (Chen et al., 2001).

3.1.2 Abnormal dendritic arborization and spine morphology of the *Cdkl5* KO mouse

Chen *et al.* reported that CDKL5 knockdown in neurons leads to abnormal dendritic arborization (Chen et al., 2010). I examined the dendritic length and branching of hippocampal CA1 pyramidal neurons by Sholl analysis using the Neurolucida system. As a result, I identified various significant differences in dendritic branching and length between the *Cdkl5* KO and control mice. Basal dendrites of the *Cdkl5* KO mice had significantly lower number of nodes and endings,

and were significantly shorter, compared to the control mice (Fig. 7D-F, I and J). Ten-um increment concentric circles from the center of soma demonstrated significantly lower number of intersections and shorter dendrites of the *Cdkl5* KO mice in the entire radii (Fig. 7G and H). As to the apical dendrites, the *Cdkl5* KO mice had similar number of nodes and endings, but had significantly decreased number of intersections and dendritic length, compared to the control (Fig. 7K-R).

Next I examined the morphology and density of dendritic spines of CA1 pyramidal neurons. In order to image the spines using laser confocal scanning microscopy, I crossed the *Cdkl5* KO mouse line with Thy1-EGFP line M transgenic mouse (Feng et al., 2000). Brain slices from Thy1-EGFP positive *Cdkl5* -/Y and +/Y mice were prepared, and the apical dendritic spines from hippocampal CA1 region were imaged. Analyses were performed using Imaris 7.4 software as described in the materials and methods. I analyzed 8,150 spines from 32 Thy1-EGFP positive *Cdkl5* +/Y (WT) neurons and 6,831 spines from 32 Thy1-EGFP positive *Cdkl5* -/Y (KO) neurons. As a result, I found that the average length of *Cdkl5* -/Y spines was increased compared to the wild-type control (WT : 0.676 μm, N=29 neurons; KO : 0.791 μm, N=32 neurons; P=2.487E-09)(Fig. 8C). The spine density per dendritic surface area was also increased in the *Cdkl5* -/Y mice (WT : 1.141/μm ^2, N=29 neurons; KO : 1.260/μm ^2, N=32 neurons; P=0.028) (Fig. 8D). Spine type classification revealed that the percentage of thin spines increased, whereas the percentage of stubby spines decreased in the *Cdkl5* KO mice (Fig. 8E). Thus the loss of CDKL5 leads to abnormal dendritic tree branching and spine morphology in the hippocampal CA1 neurons.

3.1.3 Behavioral analyses of the *Cdkl5* knockout mouse

Human patients with *CDKL5* mutations exhibit mental and behavioral abnormalities such as mental retardation, impaired motor functions, stereotypies, and sleep disturbances. These suggest critical roles of CDKL5 in motor, sensory, and emotional functions. In order to dissect the behavioral roles of CDKL5 in molecular level, I analyzed behavioral profiles of the *Cdkl5* KO mouse in collaboration with Professor Tsuyoshi Miyakawa and Associate Professor Keizo Takao, at the National Institute for Physiological Sciences.

General health, neurological screening, and motor functions of the *Cdkl5* KO mice

In general health and neurological screening test, *Cdkl5* KO mice showed no significant differences in whisker, coat, simple reflexes, grip strength (P=0.3864, Fig. 9C) and wire hang (P=0.0949, Fig. 9D), but significantly lower rectal temperature than control mice (WT: 36.391^{o}C, KO: 35.845 ^{o}C, p=0.0006, Fig. 9B).

There were no significant differences between genotypes in the hot plate test (p=0.1287, Fig. 10C) and rotarod test (p=0.2502, Fig. 10D).

Among various parameters in gait analysis, stance width of front and hind paws of the *Cdkl5* KO mice was found to be significantly shorter (front paw: P=0.0388, hind paw: P=0.0085, Fig. 11D and J). Also the stride pattern of the front paws and the angles of hind paws were found to be different (Fig. 11B and M).

There were no significant differences between genotypes in startle response to 110 dB and 120 dB acoustic stimulations (p=0.2053 and p=0.1596 respectively, Fig. 12C). There were also no differences between genotypes in all prepulse inhibition (74-110 p=0.7529, 78-110 p=0.3962, 74-120 p=0.9483, 78-120 p=0.0613, Fig. 12D).

Altered emotional responses in the *Cdkl5* KO mice

Surprisingly, I found striking alteration in emotional responses in the *Cdkl5* KO mice, by light/dark transition test, open field test, elevated plus maze test, Porsolt swim test, and tail suspension test. Light/dark test, open field test, and elevated plus maze test are well known tests used to measure anxiety-like behavior. Porsolt swim test and tail suspension test are used to measure depression-like behavior.

In light/dark transition test, *Cdkl5* KO mice showed significantly decreased distance traveled in the light chamber ($p=0.0015$, Fig. 13B), increased distance traveled in the dark chamber ($p<0.0001$, Fig. 13B), shorter time to stay in the light chamber ($p<0.0001$, Fig. 13C) and decreased number of transition between chambers ($p=0.0345$, Fig. 13D).

In open field test, *Cdkl5* KO mice showed significantly decreased traveled distance ($p=0.003$, Fig. 14B), time spent in the center ($p=0.0203$, Fig. 14D) and stereotypic counts ($p=0.019$, Fig. 14E) in the last 30 minutes of tests, and significantly decreased vertical activity ($p<0.0001$, Fig. 14C) in the last 60 minutes of tests.

In elevated plus maze test, *Cdkl5* KO mice showed significantly decreased number of entries into all arms ($p=0.0002$, Fig. 15B), decreased distance traveled ($p=0.0008$, Fig. 15D), shorter time spent on open arms ($p=0.0496$, Fig. 15E). There were no differences between genotypes in number of entries into open arms ($p=0.9119$, Fig. 15C).

These data consistently indicate that *Cdkl5* KO mice exhibit significantly increased anxiety-like behavior.

In Porsolt forced swim test, there were no differences between genotypes in immobility in second day ($p=0.0672$, Fig. 16B) and distance traveled in both first

(p=0.1442, Fig. 16C) and second days (p=0.392, Fig. 16C). But, *Cdkl5* KO mice showed significantly decreased immobility in first day (p<0.0001, Fig. 16B).

In tail suspension test, *Cdkl5* KO mice showed significantly increased immobility (p=0.0105, Fig. 16E).

These data indicate that *Cdkl5* KO mice have significant emotional abnormality.

Modulated social behaviors in the *Cdkl5* KO mice

In order to evaluate social behaviors of the *Cdkl5* KO mice, I conducted social interaction test in a novel environment (one chamber social interaction test), Crawley's sociability and social novelty preference test, and 24-hour home cage monitoring.

In social interaction test in novel environment, *Cdkl5* KO mice showed significantly increased mean duration per contact (p<0.0001, Fig. 17B), increased total duration of contacts (p=0.008, Fig. 17C), decreased number of contacts (p<0.0001, Fig. 17D), decreased total duration of active contacts (p=0.0007, Fig. 17E) and decreased distance traveled (p<0.0001, Fig. 17F).

Increased mean duration per contact (Fig. 17B) indicates that the *Cdkl5* KO mice prefer to stay together. Decreased number of contacts (Fig. 17D) and decreased total duration of active contacts (Fig. 17E) may appear to contradict the increased mean duration per contact, but this can be explained by the hypoactivity of the *Cdkl5* KO mice (Fig. 17 F).

In Crawley's sociability and social novelty preference test, preference of the mice can be quantified based on the time spent around a wire cage containing a stranger mouse vs. an empty cage in the sociability test, and stranger mouse vs. a familiar mouse

in the social novelty preference test, thus allowing assessment of social interaction from two aspects (Moy et al., 2004). Analyses of various parameters from this test revealed that the *Cdkl5* KO mice showed significantly decreased traveled distance (P=0.0001, Fig. 18B left) and preference for the center chamber (Fig. 18D right) in the first session. But these differences disappeared in the second session (Fig. 18 C and E). From these observations, these phenotypes of the KO mice could be due to heightened anxiety in the novel environment. No significant differences in other parameters between genotypes were observed (Fig. 18E – K).

Twenty-four hour monitoring in the home cage was conducted for 1 week to analyze social interaction as well as circadian activities of mice. *Cdkl5* KO mice spent significantly more time contacting with each other than WT, especially during the daytime (P=0.0012, whole day; P<0.0001 daytime, Fig. 19A top). The KO mice also showed decreased activity level during the daytime (P=0.0004, Fig. 19A bottom), but not during the night time (P=0.1535, Fig. 19A bottom).

Thus, considered collectively, social behaviors of the *Cdkl5* KO mice were modulated. Whether sociability per se of the KO mice is impaired, or these behavioral changes are mainly due to altered emotional responses, are still to be determined.

Impaired context memory in the *Cdkl5* KO mice

In order to analyze spatial context memory and cued memory of the *Cdkl5* KO mice, contextual and cued fear conditioning, and passive avoidance test were applied.

Each mouse was assessed for contextual and cued fear conditioning at 1 day and 7 days after exposure to a footshock paired with auditory-conditioned stimulus. To examine shock sensitivity, distance traveled was measured when the footshock was

delivered. Although WT and *Cdkl5* KO mice responded to footshock, the *Cdkl5* KO mice showed significantly decreased distance traveled responding to first footshock (p=0.0158, Fig. 20B), but not second (p=0.9825, Fig. 20B) and third footshock (p=0.1034, Fig. 20B). In the conditioning phase, *Cdkl5* KO mice showed significantly decreased freezing (p=0.0001, Fig. 20C). There were no differences between genotypes in percent time freezing (p=0.4247, Fig. 20D left) and distance traveled (p=0.1704, Fig. 20E left) in the contextual test at 1 day after conditioning. In altered context with cued tone at 1 day after conditioning, there were also no differences between genotypes in percent time freezing (p=0.7801, Fig. 20D right) and distance traveled (p=0.9816, Fig. 20E right), but *Cdkl5* KO mice showed significantly high freezing (p=0.0002, Fig. 20D right) and decreased distance traveled (p=0.0038, Fig. 20E right) during pretone period.

At 7 day after conditioning as well as 1 day, there were no differences between genotypes in percent time freezing (p=0.3124, Fig. 20F left) and distance traveled (p=0.1973, Fig. 20G left) in the contextual test and percent time freezing (p=0.1486, Fig. 20F right) and distance traveled (p=0.2849, Fig. 20G right) in altered context with cued tone, but *Cdkl5* KO mice showed significantly high freezing (p=0.0006, Fig. 20F right) and decreased distance traveled (p=0.0448, Fig. 20G right) during pretone period.
Thus, these data suggest that the context memory is impaired, whereas the cued memory is preserved, in the *Cdkl5* KO mice,

In passive avoidance test, *Cdkl5* KO mice showed significantly decreased latency into the light chamber at 1 day (p=0.0011, Fig. 21A), 2 day (p=0.0055, Fig. 21B) and 8 day (p=0.0063, Fig. 21C), suggesting impaired context memory.

Impaired long term reference memory and working memory in the *Cdkl5* KO mice

Barnes maze test was applied to analyze reference memory and preservation of the *Cdkl5* KO mice. During the training period, *Cdkl5* KO mice showed significantly greater number of error ($p<0.0001$, Fig. 22B), latency ($p<0.0001$, Fig. 22C) and distance ($p<0.0001$, Fig. 22D) to the target hole than WT mice. But *Cdkl5* KO mice were able to learn the target hole during the training period by overtraining, as indicated by a progressive reduction in the number of errors.

In the first probe test performed 24 hours after the 12th training, *Cdkl5* KO mice spent significantly less time around the target hole than WT mice (WT vs KO, $p=0.0009$, Fig. 22E), spending to the similar extent around the next hole (target vs next hole, $p=0.1869$, Fig. 22E). I performed additional 9 training trials till *Cdkl5* KO mice could learn the target (overtraining). In the second probe test performed 24 hours after the 21st training, *Cdkl5* KO mice spent time around the target hole to the similar extent of WT mice (WT vs KO, $p=0.1615$, Fig. 22F).

In order to assess the long–term memory, I performed third probe test after 30 days retention. In the third probe test, *Cdkl5* KO mice spent significantly less time around the target hole than WT mice (WT vs KO, $p=0.0167$, Fig. 22G), spending to the similar extent around the next hole (target vs next hole, $p=0.3926$, Fig. 22G).

Thus these result indicated long term reference memory and preservation were impaired in the *Cdkl5* KO mice.

T-maze test was applied to measure working memory of the *Cdkl5* KO mice. *Cdkl5* KO mice showed significantly decreased percentages of correct responses than WT mice in all 3 trials ($p=0.0003$, Fig. 23B). This result indicated working memory was impaired in the *Cdkl5* KO mice. Twelve *Cdkl5* KO mice out of total 22 KO mice

were not able to finish 10 trials in 50 minutes. All 22 WT mice were able to finish 10 trials in 50 minutes. Thus, *Cdkl5* KO mice spent significantly longer time to finish 10 trials than WT mice (p=0.0119, Fig. 23C). There were no significant differences between genotypes in distance traveled (p=0.4174, Fig. 23D).

3.1.4 Enhanced seizure susceptibility of the *Cdkl5* KO mouse in response to NMDA

Human patients with *CDKL5* mutations develop epilepsies, most of which are intractable infantile spasms. I anticipated that the *Cdkl5* KO mouse could be a suitable model to study pathomechanisms of such epilepsies. To my surprise, the *Cdkl5* KO mice did not develop spontaneous seizures from infancy to adulthood. Electroencephalogram (EEG) recording did not reveal apparent seizure activity during awake and sleep (data not shown). Next I analyzed seizure susceptibility of these mice in response to various seizure-inducing drugs. Kainic acid (KA) is a well-known agonist for the kainate receptor and AMPA receptor. Pentylenetetrazol (PTZ) acts as a competitive antagonist of the $GABA_A$ receptor thereby inducing seizure activities (Huang et al., 2001). N-Methyl-D-aspartic acid (NMDA) acts as a specific agonist for the NMDA receptor mimicking the action of glutamate.

Administration of KA 20 mg/kg or 25 mg/kg to post-weaned or adult *Cdkl5* KO mice elicited seizures, but to the same extent of the WT control (Fig 25A). Similarly, PTZ administration to the *Cdkl5* KO mice induced seizures to the same extent of the WT control (Fig. 25B). However, administration of 50 mg/kg NMDA induced severe generalized tonic-clonic convulsions to all of the *Cdkl5* KO mice, whereas the same dose of NMDA induced only minor myoclonic jerks of head and neck to the WT mice. Difference in the response to NMDA was quite significant (Fig. 25C).

Thus I found that the *Cdkl5* KO mice had enhanced seizure susceptibility, specifically to NMDA.

3.1.5 GluN2B subunit is aberrantly accumulated at the postsynapses of the *Cdkl5* KO mice

Significantly enhanced seizure susceptibility in response to NMDA prompted me to analyze the postsynaptic NMDA receptors of the *Cdkl5* KO mice. I assayed the amount of glutamate receptor proteins GluN1, GluN2A, GluN2B, and the MAGUK (membrane-associated guanylate kinase) family scaffolding protein PSD-95 in hippocampi of the *Cdkl5* KO and WT mice by western blotting. No significant differences in the protein level were observed in S1 (post-nuclear) fraction and P2 (synaptosomal) fraction between the KO and WT mice (S1 fraction: Fig. 25A-D, P2 fraction: Fig. 25E-H). However, further fractionation to the PSD-1T fraction revealed the significant increase of GluN2B level, but not other receptor proteins or PSD-95 in the *Cdkl5* KO mice (Fig. 25I-L). I confirmed the similar increase of GluN2B in the PSD-1T fraction from forebrains of the *Cdkl5* KO mice (Fig. 25M, N, P). The level of GluN2A was not altered (Fig. 25O). I analyzed mRNA level of *Grin2b* gene in the cerebrums of both genotypes by RT-PCR. There was no difference in *Grin2b* mRNA expression level between two genotypes (Fig. 26A). Thus these data suggest that in the *Cdkl5* KO mice, GluN2B subunit is aberrantly accumulated at the postsynapses without changes in the total amount of protein and mRNA level.

In order to pursue the mechanism of aberrant postsynaptic localization of GluN2B, I analyzed another MAGUK family scaffolding protein SAP102. SAP102 has been shown to regulate synaptic trafficking of glutamate receptors, with preference

to GluN2B (Chen et al., 2011; Muller et al., 1996; Sans et al., 2000; Standley et al., 2012). Western blotting of SAP102 normalized by PSD-95 revealed no differences in S1 (Fig. 27A - C) and P2 (Fig. 27D - F) fraction between two genotypes, but significant increase in the PSD-1T fraction from hippocampi (Fig. 27 G -I) and cerebrum (Fig. 27 J - L) of the *Cdkl5* KO mice. There were no significant differences in mRNA level in Dlg3 transcripts between two genotypes (Fig. 26B and C). Thus these data suggest that GluN2B subunit seems to be recruited at the postsynapses by accumulated SAP102 in the *Cdkl5* KO mice.

4. Discussion

In this thesis research, I analyzed the phenotypes of the *Cdkl5* KO mice and identified various behavioral abnormalities similar to human patients, impairment in dendritic arborization and spine morphology, hyperexcitability in response to NMDA, and aberrant accumulation of GluN2B subunit protein at the postsynaptic density.

4.1 Phenotypic comparison between human patients with *CDKL5* mutations and the *Cdkl5* KO mice

Human *CDKL5* gene is a member of the *Cyclin-dependent kinase-like (CDKL)* family consisting of *CDKL1*, *CDKL2*, *CDKL3*, *CDKL4*, and *CDKL5*. This gene family is conserved between human and mouse. The mouse ortholog, *Cdkl5*, has a very high sequence similarity to the human *CDKL5*, and particularly is 100% identical in the kinase domain.

Pathological mutations in the *CDKL5* gene are speculated to cause disease phenotypes by the loss-of-function (LOF) mechanisms, because most missense mutations cluster within the N-terminal kinase domain and lead to impairment of the kinase activity, and other types of mutations are thought to result in premature termination codon leading to the loss of protein due to nonsense-mediated mRNA decay. Thus the *Cdkl5* KO mouse can be regarded to model human pathology caused by the *CDKL5* mutations.

Human patients with *CDKL5* mutations exhibit various mental and behavioral phenotypes such as mental retardation, stereotypies, heightened anxiety and fear, poor social interaction, and sleep disturbances (Bahi-Buisson and Bienvenu, 2012; Willemsen et al., 2012). In this research, I identified various unique phenotypes of the

Cdkl5 KO mice. Comparing them with the symptoms of human patients, heightened anxiety, altered social interaction, seizure susceptibility, and impaired memory are observed in common. These suggest that underlying pathological mechanism by the LOF of CDKL5 is similar between humans and mice. However, differences in the LOF phenotypes also exist. Seizure susceptibility and memory impairment in the KO mice appear to be milder than those of human patients. Another difference between human patients and the KO mice lies in the muscle tonus. Most patients with *CDKL5* mutations are reported to exhibit muscular hypotonus, but the *Cdkl5* KO mice show no significant abnormality in the muscular tonus and strength. The mechanism of these differences are unsolved, but could be caused by species difference and possible functional compensation by other genes such as other *Cdkl* family members in the *Cdkl5* KO mice. Analyzing the *Cdkl2* or *Cdkl3* KO, as well as *Cdkl2/Cdkl5* or *Cdkl3/Cdkl5* double KO mice should aid elucidating the mechanisms.

4.2 Emotional functions, social behaviors, and learning/memory are impaired in the *Cdkl5* KO mouse

Our *Cdkl5* KO mice display emotional alteration such as heightened anxiety, modulated depression, modulated social interaction, and impaired learning/memory. These indicate critical roles of CDKL5 in mental, emotional, and learning/memory functions.

One of the marked characteristics of the *Cdkl5* KO mice is their significantly enhanced anxiety-like behavior. Light/dark transition test, open field test, and elevated plus maze test are 3 major behavioral tests to screen anxiety and fear of rodents. The *Cdkl5* KO mice consistently display significant anxiety-like behaviors in all 3 tests and

were confirmed to be highly anxious in nature.

However, Wang *et al.* reported that mice lacking *Cdkl5* showed decreased anxiety, autistic-like social behavior and impaired learning and memory (Wang et al., 2012). Discrepancy in emotional responses between our *Cdkl5* KO mice and their *Cdkl5* KO mice can arise from the behavioral test protocols used. Unlike us, Wang *et al.* applied only zero maze test to examine anxiety-like behavior. For measuring social behavior, both groups performed three chamber social interaction test, but I used one familiar mouse and one unfamiliar mouse, whereas they used one novel object and one unfamiliar mouse. Because of these critical differences in the protocol, the outcomes cannot be simply compared. The same tests under the same conditions should be applied to compare behavioral profiles of these two KO mouse models.

Molecular mechanisms of enhanced anxiety and fear by the loss of CDKL5 remain to be elucidated. Several brain structures are implicated in the regulation of anxiety and fear, including the amygdala, medial prefrontal cortex (mPFC), thalamus, hippocampus, and the bed nucleus of stria terminalis (Barkus et al., 2010; Davis, 2002; Uys et al., 2003). These structures of the *Cdkl5* KO mice should be investigated. Recent studies with genetically modified mice have shown that GluN1 subunit deletion specifically from the dentate gyrus not only impairs short-term spatial memory but also reduces anxiety (Niewoehner et al., 2007). In our analyses on fear conditioning, context memory was impaired but not the amygdala-dependent cued memory, suggesting the functional impairment in hippocampus. Aberrantly accumulated postsynaptic GluN2B and alterations in electrophysiological property of the NMDA receptor in the hippocampus (Prof. Toshiya Manabe and Dr. Shizuka Kobayashi, unpublished) suggest that highly enhanced anxiety may be related to impaired

hippocampal NMDA receptor function (Barkus et al., 2010; Deacon et al., 2002). Further studies are needed to clarify this and elucidate the pathomechanisms of emotional disturbance due to LOF of CDKL5.

The *Cdkl5* KO mice display learning/memory impairment. Our collaborators, Prof. Toshiya Manabe and Dr. Shizuka Kobayashi at the Institute of Medical Science, The University of Tokyo, have been conducting electrophysiological analyses of the hippocampus of the *Cdkl5* KO mouse. They have shown that the Long-term potentiation (LTP) reaction of the KO mouse is abnormal in that initial potentiation and LTP are significantly enhanced (unpublished). These and other electrophysiological abnormalities in hippocampus may underlie the impaired memory functions of the *Cdkl5* KO mice.

When I performed Barnes maze test, I noticed that the *Cdkl5* KO mouse was very slow to learn, as shown by the extra amount of training required to memorize the target location, but was able to learn in the end. This slowness of learning may be due to inefficiency of the synaptic plasticity or functioning, but other emotional factors such as anxiety and fear may be related underneath. Further electrophysiological and functional studies are needed to clarify the pathomechanisms of memory impairment in the *Cdkl5* KO mice, and to elucidate the molecular roles of CDKL5 in memory functions.

These behavioral abnormalities in the *Cdkl5* KO mice also have significant implications to clinical practice on the treatment of patients with *CDKL5* mutations, because the emotional impairment in these patients can be carefully focused.

4.3 Glutamatergic signaling is impaired in the *Cdkl5* KO mouse

Cdkl5 KO mice have abnormalities in dendritic arborization, spine morphology, and postsynaptic NMDA receptors. Collectively all these lead to impaired glutamatergic signaling in the *Cdkl5* KO mice.

Previously, Chen *et al*., knocked down CDKL5 in cultured cortical neurons *in vitro* and cortical pyramidal neurons by in utero electroporation, and showed impaired dendritic arborization (Chen et al., 2010). Ricciardi *et al.*, knocked down CDKL5 in cortical pyramidal neurons by in utero electroporation and showed increased spine density, increased spine length, and decreased VGLUT1-positive puncta (Ricciardi et al., 2012). My analyses on *Cdkl5* KO mice are nearly compatible with these data. Dendritic and spine morphology is regulated by various factors, and the key determinant is a dynamic polymerization of actin cytoskeleton. Previous studies have shown that CDKL5 is required for BDNF-induced activation of Rac1 (Chen et al., 2010). Loss of CDKL5 may lead to dysregulation of actin polymerization through the LOF effects on Rho-GTPases. Further study is needed to clarify this.

What makes the *Cdkl5* KO mice quite unique is its specific accumulation of GluN2B subunit at postsynapses. Since the *Grin2b* mRNA and total protein in the post nuclear (S1) fraction are not altered, postsynaptic trafficking of GluN2B subunit must be affected. I found that the increase of GluN2B protein at PSD-1T is accompanied by SAP102 increase in this fraction. Our collaborator, Dr. Masahiro Fukaya and Prof. Hiroyuki Sakagami at Kitasato University performed immunoelectron microscopic analyses on the hippocampus of the *Cdkl5* KO mice, and confirmed significant accumulation of GluN2B and SAP102 at postsynapses, but not other subunits or PSD-95 (unpublished).

During synaptic development, NMDA subunit composition changes from

heterodimers predominantly containing GluN2B at early stage to heterodimers containing GluN2A at mature stage, and this change is accompanied by developmental shift of MAGUK family scaffolding proteins, SAP102 to PSD-95 (Groc et al., 2006; van Zundert et al., 2004). GluN2B-containing NMDA receptor differs from GluN2A-containing NMDA receptor in various properties. GluN2A-containing NMDA receptors have rapid kinetics compared with those of GluN2B-containing NMDA receptors (Monyer et al., 1994). Surface mobility of GluN2A-containing NMDA receptors is much smaller than that of GluN2B-containing ones (Groc et al., 2006). The increase in GluN2B containing NMDA receptors at postsynapse of *Cdkl5* KO mice should change electrophysiological properties and impart neurological abnormalities in these mice, such as enhanced seizure susceptibility, memory impairment, and emotional alteration.

The mechanism by which SAP102 as well as GluN2B is aberrantly accumulated at the postsynapses of the *Cdkl5* KO mice should be investigated. SAP102 interacts with Sec8, a member of the exocyst complex, suggesting an exocyst-SAP102-NMDA receptor complex is an important component of NMDA receptor trafficking (Sans et al., 2003). SAP102 also binds with mPins (mammalian homologue of *Drosophila melanogaster* partner of inscuteable) and this interaction regulates SAP102 trafficking to the plasma membrane (Sans et al., 2005). CDKL5 may phosphorylate any of these components of trafficking machinery and regulate NMDA receptor trafficking. Zhen *et al.*, have shown that SAP102 mobility depends on actin dynamics (Zheng et al., 2010). Loss of CDKL5 may modulate SAP102 mobility by affecting actin cytoskeleton. Interestingly, mutations in human *DLG3* gene, which encodes for SAP102, cause nonsyndromic X-linked mental retardation,

suggesting the neurological effects of SAP102 modulation (Tarpey et al., 2004). *CDKL5* mutations may affect mental functions of patients via the same molecular pathway of SAP102. Further studies are needed to elucidate the mechanisms of aberrant accumulation of SAP102 and GluN2B at the postsynapses, and the consequences of these in the *Cdkl5* KO mice. So far I have not quantitated other MAGUK family proteins such as SAP97, PSD93 and DLG5. Postsynaptic proteins should be comprehensively analyzed to reveal the molecular mechanisms of abnormal targeting of SAP102 and GluN2B in the *Cdkl5* KO mice.

4.4 Pathomechanism of West syndrome with *CDKL5* mutations

West syndrome (infantile spasms) is one of the most devastating epilepsies in infancy. So far, the *ARX* gene has been identified as one of the causative genes for West syndrome, and the *ARX*-related pathomechanisms involve dysfunction of GABAergic interneurons, resulting in excessive neural excitability (Mastrangelo and Leuzzi, 2012). In contrast, I have identified abnormal subunit localization and function of the NMDA receptors in the *Cdkl5* KO mouse, which implicate the gain of function of the excitatory synapses as another possible pathomechanisms of West syndrome. This novel finding should promote elucidation of pathomechanisms and treatment of West syndrome and other intractable epilepsies. If the similar accumulation of GluN2B-containig NMDA receptors occur in the postsynapses of human patients, it will lead to enhanced seizure susceptibility and neurotoxicity. Then, a possible treatment strategy for the *CDKL5*-related epilepsies must be antagonizing the GluN2B-containing NMDA receptor hyperactivity. One candidate drug for this is Felbamate, which is an allosteric antagonist at the GluN2B subunit of the NMDA

receptor, also having $GABA_A$ receptor agonist properties (Harty and Rogawski, 2000; Kleckner et al., 1999). Felbamate has already been used as an anticonvulsant agent in the United States, but is not approved in Japan. Ifenprodil is another candidate drug, since it is an NMDA receptor antagonist with selective targeting of GluN2B subunit (Williams, 1993; Williams et al., 1993). In order to provide with theoretical basis for such treatment, efficacy of these drugs should be confirmed on the *Cdkl5* KO mice. Putting all this together, this research shed light on the NMDA receptor dysfunction as underlying mechanism of the West syndrome, and must contribute to future progress of neuroscience as well as clinical practice for developmental disorders.

Acknowledgement

I greatly appreciate Associate professor Teruyuki Tanaka and Prof. Masashi Mizuguchi for proposal and supervision of the present study. I am indebted to Dr. Keizo Takao and Prof. Tsuyoshi Miyakawa for the instruction on the behavioral study. I want to thank Tamaki Kise for technical support for behavioral study in National Institute for Physiological Sciences (NIPS), and thank Kaori Takamatsu for clerical support for visiting NIPS. I am indebted to Dr. Masahiro Fukaya and Prof. Hiroyuki Sakagami for collaboration of electron microscopic study. I am indebted to Dr. Shizuka Kobayashi and Prof. Toshiya Manabe for collaboration of electrophysiological study.

I want to thank Aya Watanabe for establishing *Cdkl5* KO mice used in this study. I want to thank Mr. Yutaro Kashiwagi and Prof. Shigeo Okabe for technical advice of subcellular fractionation. I want to thank Dr. Kanzo Suzuki, Dr. Sayaka Takemoto-Kimura, Dr. Hiroyuki Okuno and Prof. Haruhiko Bito for technical advice of biochemical study. I also want to thank Dr. Yoichi Watanabe and Prof. Kiyoshi Kita for technical advice of biochemical study. I want to thank Dr. Eiki Kimura and Prof. Chiharu Tohyama for technical advice of Sholl analysis. I want to thank Dr. Sayaka Komano and Dr. Masahiro Yamaguchi for technical advice of EEG study.

This thesis research is supported by a Grant-in-Aid for Scientific Research on Innovative Areas (Comprehensive Brain Science Network) from the Ministry of Education, Science, Sports and Culture of Japan.

References

Bahi-Buisson, N., and T. Bienvenu. 2012. CDKL5-Related Disorders: From Clinical Description to Molecular Genetics. *Mol Syndromol*. 2:137-152.

Bahi-Buisson, N., A. Kaminska, N. Boddaert, M. Rio, A. Afenjar, M. Gerard, F. Giuliano, J. Motte, D. Heron, M.A. Morel, P. Plouin, C. Richelme, V. des Portes, O. Dulac, C. Philippe, C. Chiron, R. Nabbout, and T. Bienvenu. 2008a. The three stages of epilepsy in patients with CDKL5 mutations. *Epilepsia*. 49:1027-1037.

Bahi-Buisson, N., J. Nectoux, H. Rosas-Vargas, M. Milh, N. Boddaert, B. Girard, C. Cances, D. Ville, A. Afenjar, M. Rio, D. Heron, M.A. N'Guyen Morel, A. Arzimanoglou, C. Philippe, P. Jonveaux, J. Chelly, and T. Bienvenu. 2008b. Key clinical features to identify girls with CDKL5 mutations. *Brain*. 131:2647-2661.

Barkus, C., S.B. McHugh, R. Sprengel, P.H. Seeburg, J.N. Rawlins, and D.M. Bannerman. 2010. Hippocampal NMDA receptors and anxiety: at the interface between cognition and emotion. *European journal of pharmacology*. 626:49-56.

Bertani, I., L. Rusconi, F. Bolognese, G. Forlani, B. Conca, L. De Monte, G. Badaracco, N. Landsberger, and C. Kilstrup-Nielsen. 2006. Functional consequences of mutations in CDKL5, an X-linked gene involved in infantile spasms and mental retardation. *J Biol Chem*. 281:32048-32056.

Chen, B.S., E.V. Thomas, A. Sanz-Clemente, and K.W. Roche. 2011. NMDA receptor-dependent regulation of dendritic spine morphology by SAP102 splice variants. *J Neurosci*. 31:89-96.

Chen, Q., Y.C. Zhu, J. Yu, S. Miao, J. Zheng, L. Xu, Y. Zhou, D. Li, C. Zhang, J. Tao, and Z.Q. Xiong. 2010. CDKL5, a protein associated with rett syndrome, regulates neuronal morphogenesis via Rac1 signaling. *J Neurosci*. 30:12777-12786.

Chen, R.Z., S. Akbarian, M. Tudor, and R. Jaenisch. 2001. Deficiency of methyl-CpG binding protein-2 in CNS neurons results in a Rett-like phenotype in mice. *Nat Genet*. 27:327-331.

Crawley, J.N. 2007. What's Wrong With My Mouse: Behavioral Phenotyping of Transgenic and Knockout Mice, Second Edition Wiley-Liss.

Davis, M. 2002. Neural Circuitry of anxiety and stress disorders. *In* Neuropsychopharmacology: The Fifth Generation of Progress. K.L. Davis, J.T. Coyle, and C. Nemeroff, editors. American College of Neuropsychopharmacology, Washington, DC. 931–951.

Deacon, R.M., D.M. Bannerman, and J.N. Rawlins. 2002. Anxiolytic effects of

cytotoxic hippocampal lesions in rats. *Behavioral neuroscience*. 116:494-497.

Elia, M., M. Falco, R. Ferri, A. Spalletta, M. Bottitta, G. Calabrese, M. Carotenuto, S.A. Musumeci, M. Lo Giudice, and M. Fichera. 2008. CDKL5 mutations in boys with severe encephalopathy and early-onset intractable epilepsy. *Neurology*. 71:997-999.

Feng, G., R.H. Mellor, M. Bernstein, C. Keller-Peck, Q.T. Nguyen, M. Wallace, J.M. Nerbonne, J.W. Lichtman, and J.R. Sanes. 2000. Imaging neuronal subsets in transgenic mice expressing multiple spectral variants of GFP. *Neuron*. 28:41-51.

Fichou, Y., J. Nectoux, N. Bahi-Buisson, J. Chelly, and T. Bienvenu. 2011. An isoform of the severe encephalopathy-related CDKL5 gene, including a novel exon with extremely high sequence conservation, is specifically expressed in brain. *J Hum Genet*. 56:52-57.

Froyen, G., H. Van Esch, M. Bauters, K. Hollanders, S.G. Frints, J.R. Vermeesch, K. Devriendt, J.P. Fryns, and P. Marynen. 2007. Detection of genomic copy number changes in patients with idiopathic mental retardation by high-resolution X-array-CGH: important role for increased gene dosage of XLMR genes. *Hum Mutat*. 28:1034-1042.

Groc, L., M. Heine, S.L. Cousins, F.A. Stephenson, B. Lounis, L. Cognet, and D. Choquet. 2006. NMDA receptor surface mobility depends on NR2A-2B subunits. *Proceedings of the National Academy of Sciences of the United States of America*. 103:18769-18774.

Hagberg, B.A., and O.H. Skjeldal. 1994. Rett variants: a suggested model for inclusion criteria. *Pediatric neurology*. 11:5-11.

Harrison, F.E., R.S. Reiserer, A.J. Tomarken, and M.P. McDonald. 2006. Spatial and nonspatial escape strategies in the Barnes maze. *Learning & memory*. 13:809-819.

Harty, T.P., and M.A. Rogawski. 2000. Felbamate block of recombinant N-methyl-D-aspartate receptors: selectivity for the NR2B subunit. *Epilepsy research*. 39:47-55.

Huang, R.Q., C.L. Bell-Horner, M.I. Dibas, D.F. Covey, J.A. Drewe, and G.H. Dillon. 2001. Pentylenetetrazole-induced inhibition of recombinant gamma-aminobutyric acid type A (GABA(A)) receptors: mechanism and site of action. *The Journal of pharmacology and experimental therapeutics*. 298:986-995.

Kalscheuer, V.M., J. Tao, A. Donnelly, G. Hollway, E. Schwinger, S. Kubart, C. Menzel, M. Hoeltzenbein, N. Tommerup, H. Eyre, M. Harbord, E. Haan, G.R. Sutherland,

H.H. Ropers, and J. Gecz. 2003. Disruption of the serine/threonine kinase 9 gene causes severe X-linked infantile spasms and mental retardation. *American journal of human genetics*. 72:1401-1411.

Kilstrup-Nielsen, C., L. Rusconi, P. La Montanara, D. Ciceri, A. Bergo, F. Bedogni, and N. Landsberger. 2012. What we know and would like to know about CDKL5 and its involvement in epileptic encephalopathy. *Neural Plast*. 2012:728267.

Kleckner, N.W., J.C. Glazewski, C.C. Chen, and T.D. Moscrip. 1999. Subtype-selective antagonism of N-methyl-D-aspartate receptors by felbamate: insights into the mechanism of action. *The Journal of pharmacology and experimental therapeutics*. 289:886-894.

Komada, M., K. Takao, and T. Miyakawa. 2008. Elevated plus maze for mice. *Journal of visualized experiments : JoVE*.

Liang, J.S., K. Shimojima, R. Takayama, J. Natsume, M. Shichiji, K. Hirasawa, K. Imai, T. Okanishi, S. Mizuno, A. Okumura, M. Sugawara, T. Ito, H. Ikeda, Y. Takahashi, H. Oguni, M. Osawa, and T. Yamamoto. 2011. CDKL5 alterations lead to early epileptic encephalopathy in both genders. *Epilepsia*. 52:1835-1842.

Lin, C., B. Franco, and M.R. Rosner. 2005. CDKL5/Stk9 kinase inactivation is associated with neuronal developmental disorders. *Hum Mol Genet*. 14:3775-3786.

Manning, G., D.B. Whyte, R. Martinez, T. Hunter, and S. Sudarsanam. 2002. The protein kinase complement of the human genome. *Science*. 298:1912-1934.

Mari, F., S. Azimonti, I. Bertani, F. Bolognese, E. Colombo, R. Caselli, E. Scala, I. Longo, S. Grosso, C. Pescucci, F. Ariani, G. Hayek, P. Balestri, A. Bergo, G. Badaracco, M. Zappella, V. Broccoli, A. Renieri, C. Kilstrup-Nielsen, and N. Landsberger. 2005. CDKL5 belongs to the same molecular pathway of MeCP2 and it is responsible for the early-onset seizure variant of Rett syndrome. *Hum Mol Genet*. 14:1935-1946.

Mastrangelo, M., and V. Leuzzi. 2012. Genes of early-onset epileptic encephalopathies: from genotype to phenotype. *Pediatric neurology*. 46:24-31.

Matsuo, N., K. Takao, K. Nakanishi, N. Yamasaki, K. Tanda, and T. Miyakawa. 2010. Behavioral profiles of three C57BL/6 substrains. *Frontiers in behavioral neuroscience*. 4:29.

Miyakawa, T., L.M. Leiter, D.J. Gerber, R.R. Gainetdinov, T.D. Sotnikova, H. Zeng, M.G. Caron, and S. Tonegawa. 2003. Conditional calcineurin knockout mice exhibit multiple abnormal behaviors related to schizophrenia. *Proceedings of the National Academy of Sciences of the United States of America*. 100:8987-8992.

Miyakawa, T., E. Yared, J.H. Pak, F.L. Huang, K.P. Huang, and J.N. Crawley. 2001. Neurogranin null mutant mice display performance deficits on spatial learning tasks with anxiety related components. *Hippocampus*. 11:763-775.

Montini, E., G. Andolfi, A. Caruso, G. Buchner, S.M. Walpole, M. Mariani, G. Consalez, D. Trump, A. Ballabio, and B. Franco. 1998. Identification and characterization of a novel serine-threonine kinase gene from the Xp22 region. *Genomics*. 51:427-433.

Monyer, H., N. Burnashev, D.J. Laurie, B. Sakmann, and P.H. Seeburg. 1994. Developmental and regional expression in the rat brain and functional properties of four NMDA receptors. *Neuron*. 12:529-540.

Moy, S.S., J.J. Nadler, A. Perez, R.P. Barbaro, J.M. Johns, T.R. Magnuson, J. Piven, and J.N. Crawley. 2004. Sociability and preference for social novelty in five inbred strains: an approach to assess autistic-like behavior in mice. *Genes, brain, and behavior*. 3:287-302.

Muller, B.M., U. Kistner, S. Kindler, W.J. Chung, S. Kuhlendahl, S.D. Fenster, L.F. Lau, R.W. Veh, R.L. Huganir, E.D. Gundelfinger, and C.C. Garner. 1996. SAP102, a novel postsynaptic protein that interacts with NMDA receptor complexes in vivo. *Neuron*. 17:255-265.

Nemos, C., L. Lambert, F. Giuliano, B. Doray, A. Roubertie, A. Goldenberg, B. Delobel, V. Layet, A. N'Guyen M, A. Saunier, F. Verneau, P. Jonveaux, and C. Philippe. 2009. Mutational spectrum of CDKL5 in early-onset encephalopathies: a study of a large collection of French patients and review of the literature. *Clinical genetics*. 76:357-371.

Neul, J.L., W.E. Kaufmann, D.G. Glaze, J. Christodoulou, A.J. Clarke, N. Bahi-Buisson, H. Leonard, M.E. Bailey, N.C. Schanen, M. Zappella, A. Renieri, P. Huppke, A.K. Percy, and C. RettSearch. 2010. Rett syndrome: revised diagnostic criteria and nomenclature. *Annals of neurology*. 68:944-950.

Niewoehner, B., F.N. Single, O. Hvalby, V. Jensen, S. Meyer zum Alten Borgloh, P.H. Seeburg, J.N. Rawlins, R. Sprengel, and D.M. Bannerman. 2007. Impaired spatial working memory but spared spatial reference memory following functional loss of NMDA receptors in the dentate gyrus. *The European journal of neuroscience*. 25:837-846.

Ricciardi, S., C. Kilstrup-Nielsen, T. Bienvenu, A. Jacquette, N. Landsberger, and V. Broccoli. 2009. CDKL5 influences RNA splicing activity by its association to the nuclear speckle molecular machinery. *Hum Mol Genet*. 18:4590-4602.

Ricciardi, S., F. Ungaro, M. Hambrock, N. Rademacher, G. Stefanelli, D. Brambilla, A.

Sessa, C. Magagnotti, A. Bachi, E. Giarda, C. Verpelli, C. Kilstrup-Nielsen, C. Sala, V.M. Kalscheuer, and V. Broccoli. 2012. CDKL5 ensures excitatory synapse stability by reinforcing NGL-1-PSD95 interaction in the postsynaptic compartment and is impaired in patient iPSC-derived neurons. *Nature cell biology*. 14:911-923.

Rusconi, L., L. Salvatoni, L. Giudici, I. Bertani, C. Kilstrup-Nielsen, V. Broccoli, and N. Landsberger. 2008. CDKL5 expression is modulated during neuronal development and its subcellular distribution is tightly regulated by the C-terminal tail. *J Biol Chem*. 283:30101-30111.

Sakai, K., and J. Miyazaki. 1997. A transgenic mouse line that retains Cre recombinase activity in mature oocytes irrespective of the cre transgene transmission. *Biochem Biophys Res Commun*. 237:318-324.

Sans, N., R.S. Petralia, Y.X. Wang, J. Blahos, 2nd, J.W. Hell, and R.J. Wenthold. 2000. A developmental change in NMDA receptor-associated proteins at hippocampal synapses. *J Neurosci*. 20:1260-1271.

Sans, N., K. Prybylowski, R.S. Petralia, K. Chang, Y.X. Wang, C. Racca, S. Vicini, and R.J. Wenthold. 2003. NMDA receptor trafficking through an interaction between PDZ proteins and the exocyst complex. *Nature cell biology*. 5:520-530.

Sans, N., P.Y. Wang, Q. Du, R.S. Petralia, Y.X. Wang, S. Nakka, J.B. Blumer, I.G. Macara, and R.J. Wenthold. 2005. mPins modulates PSD-95 and SAP102 trafficking and influences NMDA receptor surface expression. *Nature cell biology*. 7:1179-1190.

Shin, E., Y. Kashiwagi, T. Kuriu, H. Iwasaki, T. Tanaka, H. Koizumi, J.G. Gleeson, and S. Okabe. 2013. Doublecortin-like kinase enhances dendritic remodelling and negatively regulates synapse maturation. *Nature communications*. 4:1440.

Shoji, H., H. Hagihara, K. Takao, S. Hattori, and T. Miyakawa. 2012. T-maze forced alternation and left-right discrimination tasks for assessing working and reference memory in mice. *Journal of visualized experiments : JoVE*.

Standley, S., R.S. Petralia, M. Gravell, R. Hamilton, Y.X. Wang, M. Schubert, and [Chen, R. J. 2012. Trafficking of the NMDAR2B receptor subunit distal cytoplasmic tail from endoplasmic reticulum to the synapse. *PloS one*. 7:e39585.

Takao, K., and T. Miyakawa. 2006. Light/dark transition test for mice. *Journal of visualized experiments : JoVE*:104.

Takao, K., and T. Miyakawa. 2009. Intrauterine environment-genome interaction and children's development (4): Brain-behavior phenotypying of genetically-engineered mice using a comprehensive behavioral test battery on

research of neuropsychiatric disorders. *The Journal of toxicological sciences*. 34 Suppl 2:SP293-305.

Takao, K., K. Tanda, K. Nakamura, J. Kasahara, K. Nakao, M. Katsuki, K. Nakanishi, N. Yamasaki, K. Toyama, M. Adachi, M. Umeda, T. Araki, K. Fukunaga, H. Kondo, H. Sakagami, and T. Miyakawa. 2010. Comprehensive behavioral analysis of calcium/calmodulin-dependent protein kinase IV knockout mice. *PloS one*. 5:e9460.

Takao, K., K. Toyama, K. Nakanishi, S. Hattori, H. Takamura, M. Takeda, T. Miyakawa, and R. Hashimoto. 2008. Impaired long-term memory retention and working memory in sdy mutant mice with a deletion in Dtnbp1, a susceptibility gene for schizophrenia. *Molecular brain*. 1:11.

Tanda, K., A. Nishi, N. Matsuo, K. Nakanishi, N. Yamasaki, T. Sugimoto, K. Toyama, K. Takao, and T. Miyakawa. 2009. Abnormal social behavior, hyperactivity, impaired remote spatial memory, and increased D1-mediated dopaminergic signaling in neuronal nitric oxide synthase knockout mice. *Molecular brain*. 2:19.

Tarpey, P., J. Parnau, M. Blow, H. Woffendin, G. Bignell, C. Cox, J. Cox, H. Davies, S. Edkins, S. Holden, A. Korny, U. Mallya, J. Moon, S. O'Meara, A. Parker, P. Stephens, C. Stevens, J. Teague, A. Donnelly, M. Mangelsdorf, J. Mulley, M. Partington, G. Turner, R. Stevenson, C. Schwartz, I. Young, D. Easton, M. Bobrow, P.A. Futreal, M.R. Stratton, J. Gecz, R. Wooster, and F.L. Raymond. 2004. Mutations in the DLG3 gene cause nonsyndromic X-linked mental retardation. *American journal of human genetics*. 75:318-324.

Tzschach, A., W. Chen, F. Erdogan, A. Hoeller, H.H. Ropers, C. Castellan, R. Ullmann, and A. Schinzel. 2008. Characterization of interstitial Xp duplications in two families by tiling path array CGH. *Am J Med Genet A*. 146A:197-203.

Uys, J.D., D.J. Stein, W.M. Daniels, and B.H. Harvey. 2003. Animal models of anxiety disorders. *Current psychiatry reports*. 5:274-281.

van Zundert, B., A. Yoshii, and M. Constantine-Paton. 2004. Receptor compartmentalization and trafficking at glutamate synapses: a developmental proposal. *Trends in neurosciences*. 27:428-437.

Wang, I.T., M. Allen, D. Goffin, X. Zhu, A.H. Fairless, E.S. Brodkin, S.J. Siegel, E.D. Marsh, J.A. Blendy, and Z. Zhou. 2012. Loss of CDKL5 disrupts kinome profile and event-related potentials leading to autistic-like phenotypes in mice. *Proceedings of the National Academy of Sciences of the United States of America*. 109:21516-21521.

Westmark, C.J., P.R. Westmark, A.M. Beard, S.M. Hildebrandt, and J.S. Malter. 2008. Seizure susceptibility and mortality in mice that over-express amyloid precursor protein. *International journal of clinical and experimental pathology*. 1:157-168.

Willemsen, M.H., J.H. Rensen, H.M. van Schrojenstein-Lantman de Valk, B.C. Hamel, and T. Kleefstra. 2012. Adult Phenotypes in Angelman- and Rett-Like Syndromes. *Mol Syndromol*. 2:217-234.

Williams, K. 1993. Ifenprodil discriminates subtypes of the N-methyl-D-aspartate receptor: selectivity and mechanisms at recombinant heteromeric receptors. *Molecular pharmacology*. 44:851-859.

Williams, K., S.L. Russell, Y.M. Shen, and P.B. Molinoff. 1993. Developmental switch in the expression of NMDA receptors occurs in vivo and in vitro. *Neuron*. 10:267-278.

Williamson, S.L., L. Giudici, C. Kilstrup-Nielsen, W. Gold, G.J. Pelka, P.P. Tam, A. Grimm, D. Prodi, N. Landsberger, and J. Christodoulou. 2012. A novel transcript of cyclin-dependent kinase-like 5 (CDKL5) has an alternative C-terminus and is the predominant transcript in brain. *Hum Genet*. 131:187-200.

Wu, G., Z.H. Lu, J. Wang, Y. Wang, X. Xie, M.F. Meyenhofer, and R.W. Ledeen. 2005. Enhanced susceptibility to kainate-induced seizures, neuronal apoptosis, and death in mice lacking gangliotetraose gangliosides: protection with LIGA 20, a membrane-permeant analog of GM1. *J Neurosci*. 25:11014-11022.

Yao, I., K. Takao, T. Miyakawa, S. Ito, and M. Setou. 2011. Synaptic E3 ligase SCRAPPER in contextual fear conditioning: extensive behavioral phenotyping of Scrapper heterozygote and overexpressing mutant mice. *PloS one*. 6:e17317.

Zheng, C.Y., R.S. Petralia, Y.X. Wang, B. Kachar, and R.J. Wenthold. 2010. SAP102 is a highly mobile MAGUK in spines. *J Neurosci*. 30:4757-4766.

Zhu, Y.C., D. Li, L. Wang, B. Lu, J. Zheng, S.L. Zhao, R. Zeng, and Z.Q. Xiong. 2013. Palmitoylation-dependent CDKL5-PSD-95 interaction regulates synaptic targeting of CDKL5 and dendritic spine development. *Proceedings of the National Academy of Sciences of the United States of America*. 110:9118-9123.

	Test	Measurement
1	General health/neurological screen	body weight, rectal temperature, whisker, coat, simple reflexes
2	Wire hang	muscle strength
3	Grip strength test	muscle strength
4	Gait analysis	gait, locomotion, motor function
5	Hot plate test	nociception
6	Rotarod	motor coordination
7	Startle response & prepulse inhibition	sensory-motor gating
8	Light/dark transition	anxiety-like behavior
9	Open Field	activity, anxiety-like behavior
10	Elevated plus maze	anxiety-like behavior
11	Social interaction (novel environment)	social behavior
12	Social interaction (Crawley)	social behavior
13	24-hr home cage monitoring	24-hr activity, social behavior
14	Porsolt Forced Swim	depression-like behavior
15	Tail suspension	depression-like behavior
16	Contextual and cued fear conditioning	context memory
17	Passive avoidance	context memory
18	Barnes maze	reference memory, preservation,
19	T-maze	working memory
20	Y-maze	working memory

Table 1.

Comprehensive behavioral test battery which I conducted.

Modified from (Takao and Miyakawa, 2009).

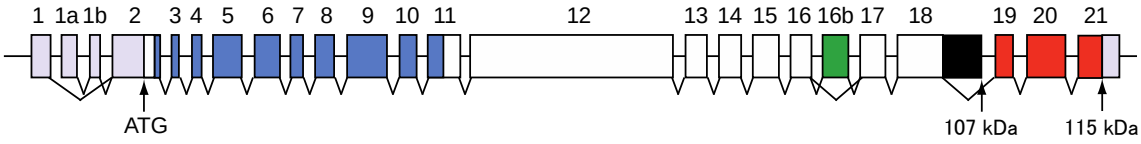

Figure 1. Structure of the *CDKL5* gene

The human *CDKL5* gene consists of 24 exons. Translation starts in exon 2, and terminates in intron 18 (107 kDa isoform) or in exon 21 (115 kDa isoform) by alternative splicing. An additional splice variant containing exon 16b is generated. Exons in gray, blue, and white indicates untranslated regions, kinase domain, and common C-terminal region, respectively. Exons in green, black, and red indicate isoform–specific sequences. Exon lengths are illustrated in scale.
Modified from (Kilstrup-Nielsen et al., 2012).

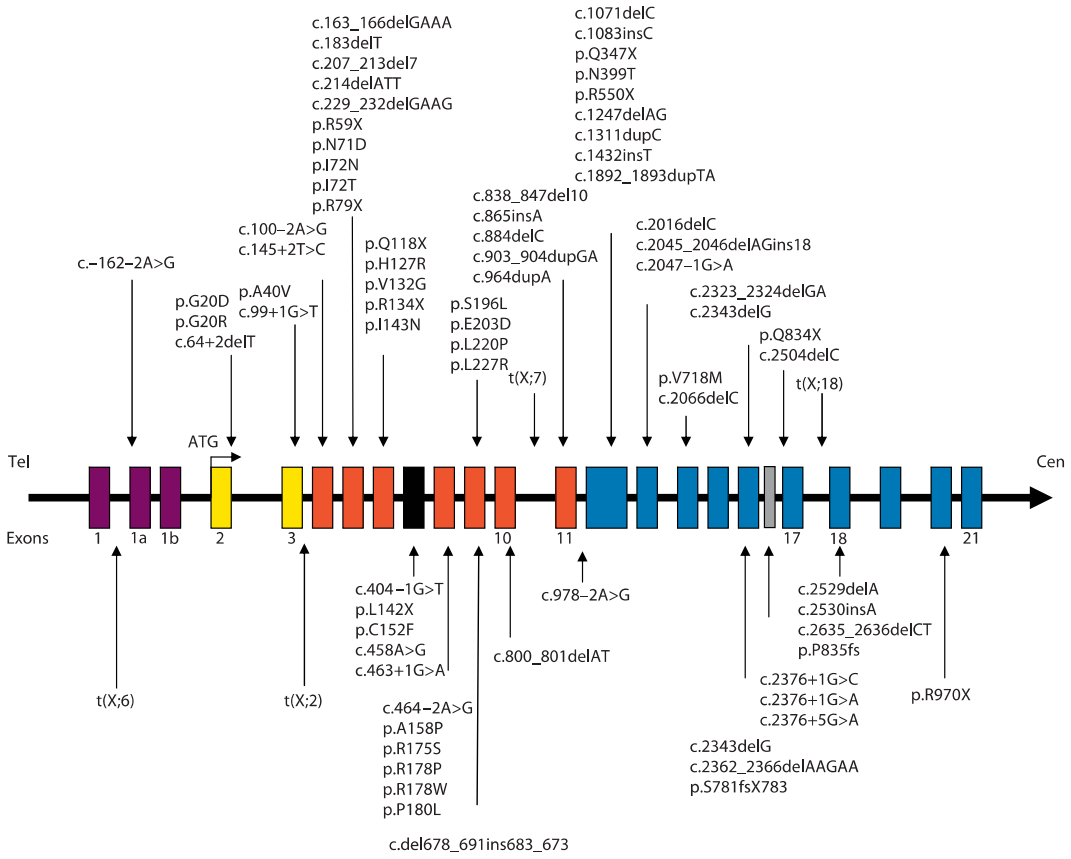

Bahi-Buisson et al., 2012

Figure 2. Reported point mutations and translocations of *CDKL5* gene

All except one (p.V718M) missense mutations cluster within exons 2-11.

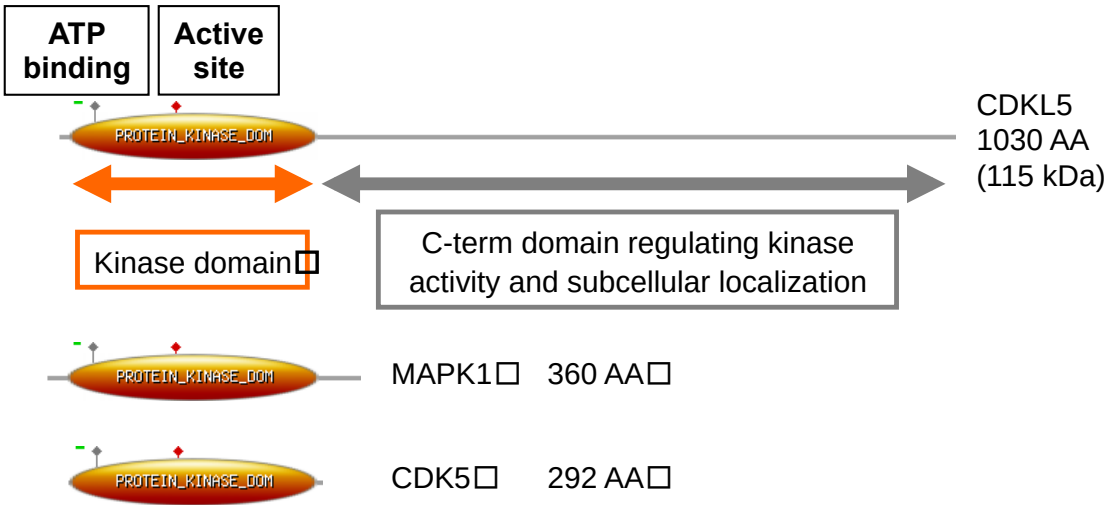

Figure 3. CDKL5 protein

The CDKL5 protein harbors an N-terminal serine/threonine kinase domain (AA 13-297), which is homologous to MAPK1 or CDK5. C-terminal domain regulates its kinase activity and subcellular localization.

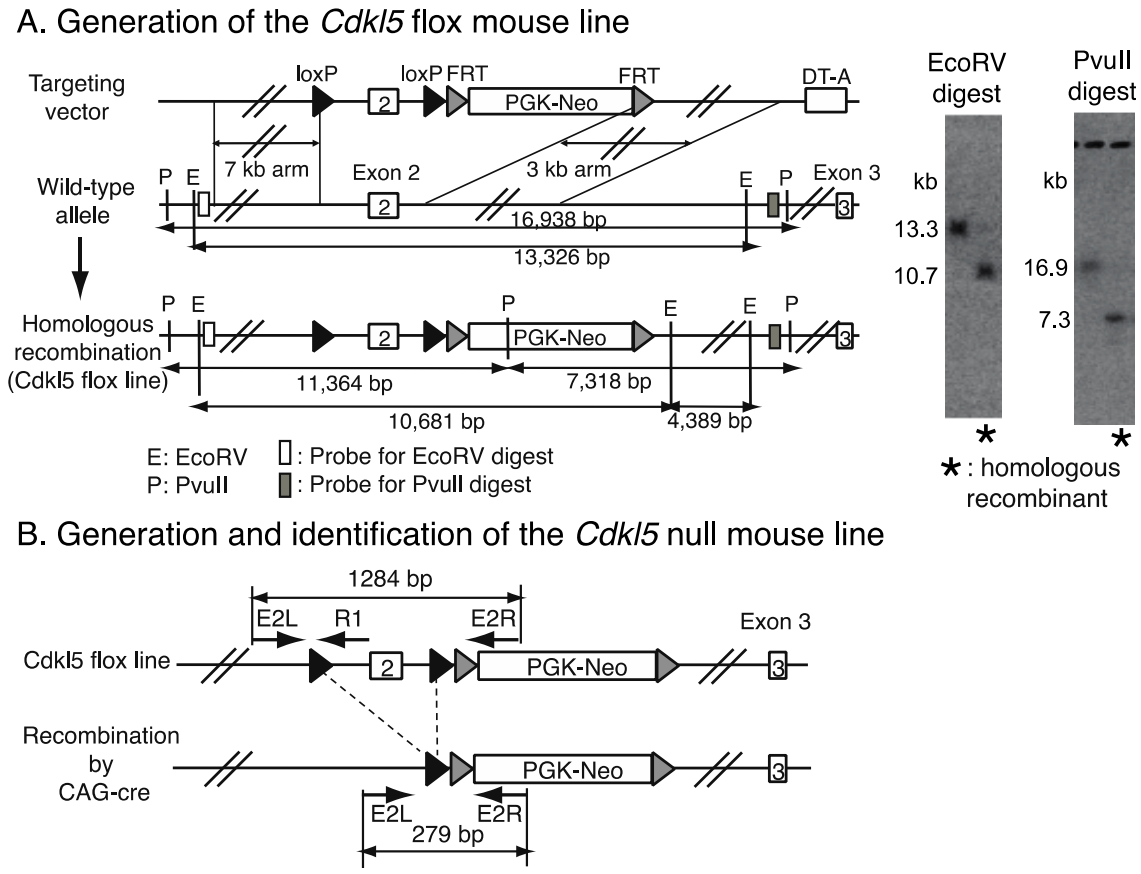

Figure 4. Targeting constructs of the *Cdkl5* flox mouse and null mouse

A. Targeting construct of the *Cdkl5* flox mouse. Exon 2 of *Cdkl5* gene was flanked by two loxP sites (left). Homologous recombination was confirmed by southern blotting (right).

B. By crossing *Cdkl5* flox/Y male mouse with CAG-*cre* transgenic female mouse, which mediate the site-specific recombination of paternally derived target gene upon fertilization, *Cdkl5* heterozygous and hemizygous knockout mice were successfully obtained.

C. Confirmation of deletion of CDKL5 in the mutant mice by western blotting. *Cdkl5* hemizygous knockout mice showed absence of CDKL5, and *Cdkl5* heterozygous mice showed approximately half the amount of CDKL5.

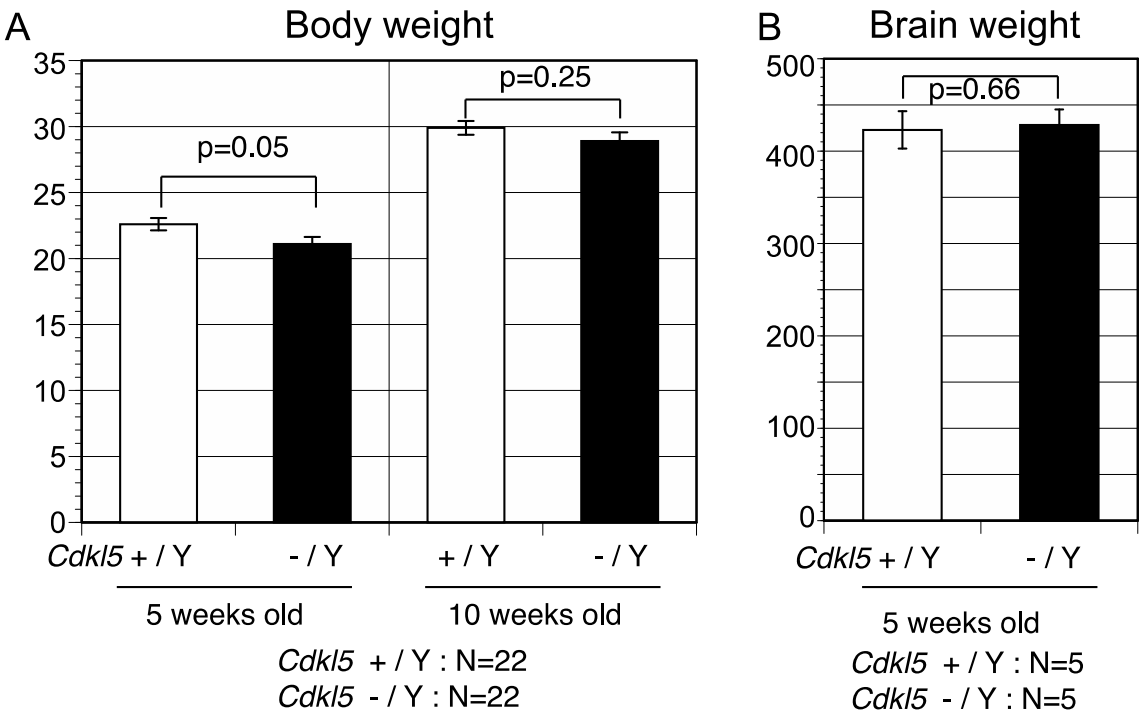

Figure 5. Body weight and brain weight of the *Cdkl5* KO mouse

A. Averaged body weight of the *Cdkl5* KO mice (5 and 10 weeks of age).
There are no statistical differences between *Cdkl5* -/Y and +/Y mice.

B. Averaged brain weight of the *Cdkl5* KO mice (5 weeks of age)
There is no statistical difference between *Cdkl5* -/Y and +/Y mice.

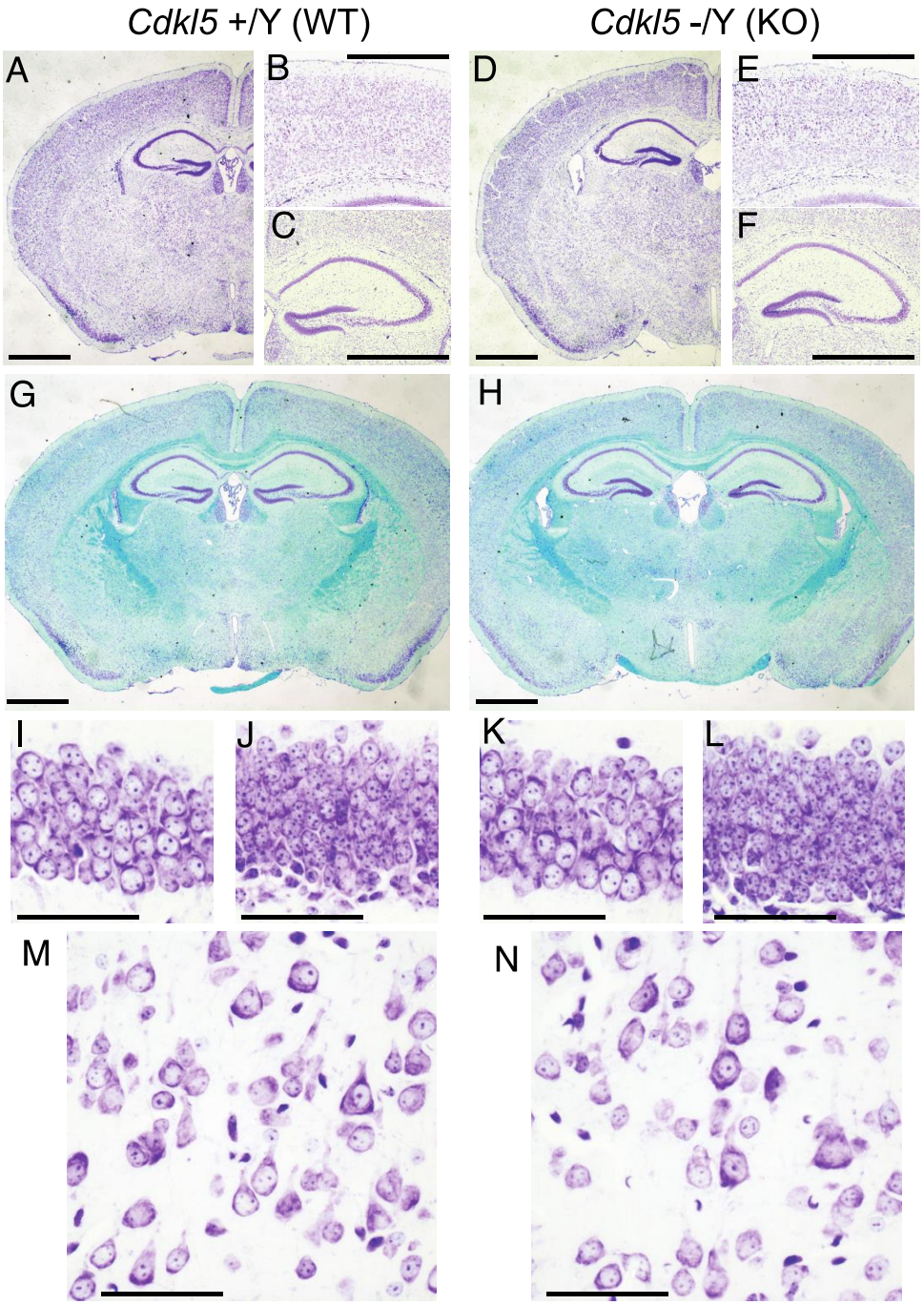

Figure 6. No gross abnormalities of the *Cdkl5* KO mouse brain at postnatal day 21.

Scale bars: A – H 1 mm, I – N 50 um.

A – F. Nissl staining of the mouse brains.

Nissl staining of the wild type mouse whole brain (A), cortex (B) and hippocampus (C). Nissl staining of the *Cdkl5* KO mouse whole brain (D), cortex (E) and hippocampus (F).

There are no gross anatomical abnormalities in the *Cdkl5* KO mouse brain.

G – H. Klüver–Barrera (KB) staining of the wild type (G) and *Cdkl5* KO mouse brain (H). There is no abnormality in the myelination between the wild type and *Cdkl5* KO mice.

I – N. Comparison of neuronal cell size and nuclear size by Nissl staining.
Hippocampal CA1 pyramidal neurons in the wild type (I) and *Cdkl5* KO mice (K). Neurons in dentate gyrus in the wild type (J) and *Cdkl5* KO mice (L). Neurons in somatosensory cortex in the wild type (M) and *Cdkl5* KO mice (N). There are no abnormalities in the cell and nuclear size between the wild type and *Cdkl5* KO mice.

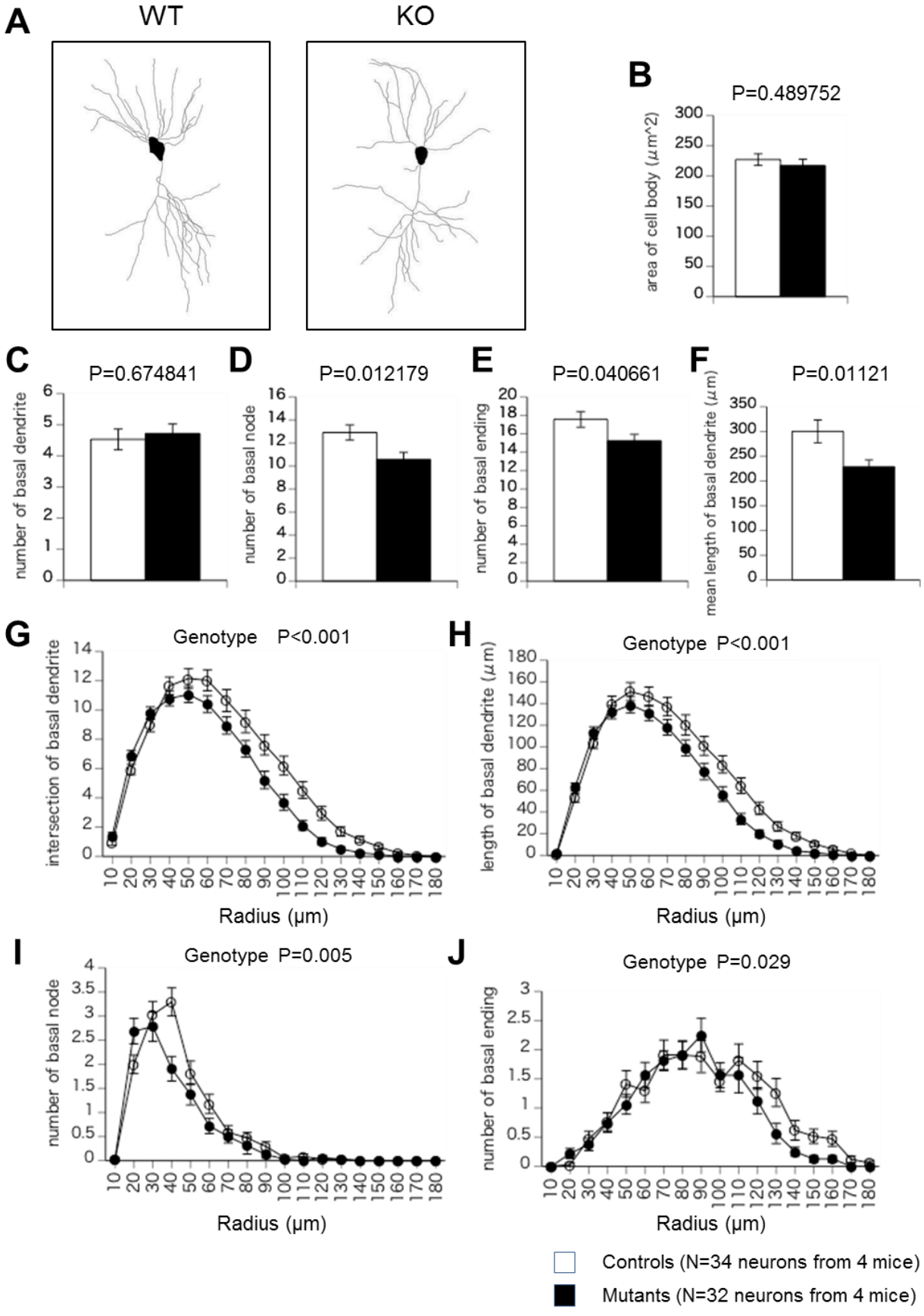
A
WT
KO
B
P=0.489752
area of cell body (μm^2)
C
P=0.674841
number of basal dendrite
D
P=0.012179
number of basal node
E
P=0.040661
number of basal ending
F
P=0.01121
mean length of basal dendrite (μm)
G
Genotype P<0.001
intersection of basal dendrite
Radius (μm)
H
Genotype P<0.001
length of basal dendrite (μm)
Radius (μm)
I
Genotype P=0.005
number of basal node
Radius (μm)
J
Genotype P=0.029
number of basal ending
Radius (μm)
Controls (N=34 neurons from 4 mice)
Mutants (N=32 neurons from 4 mice)

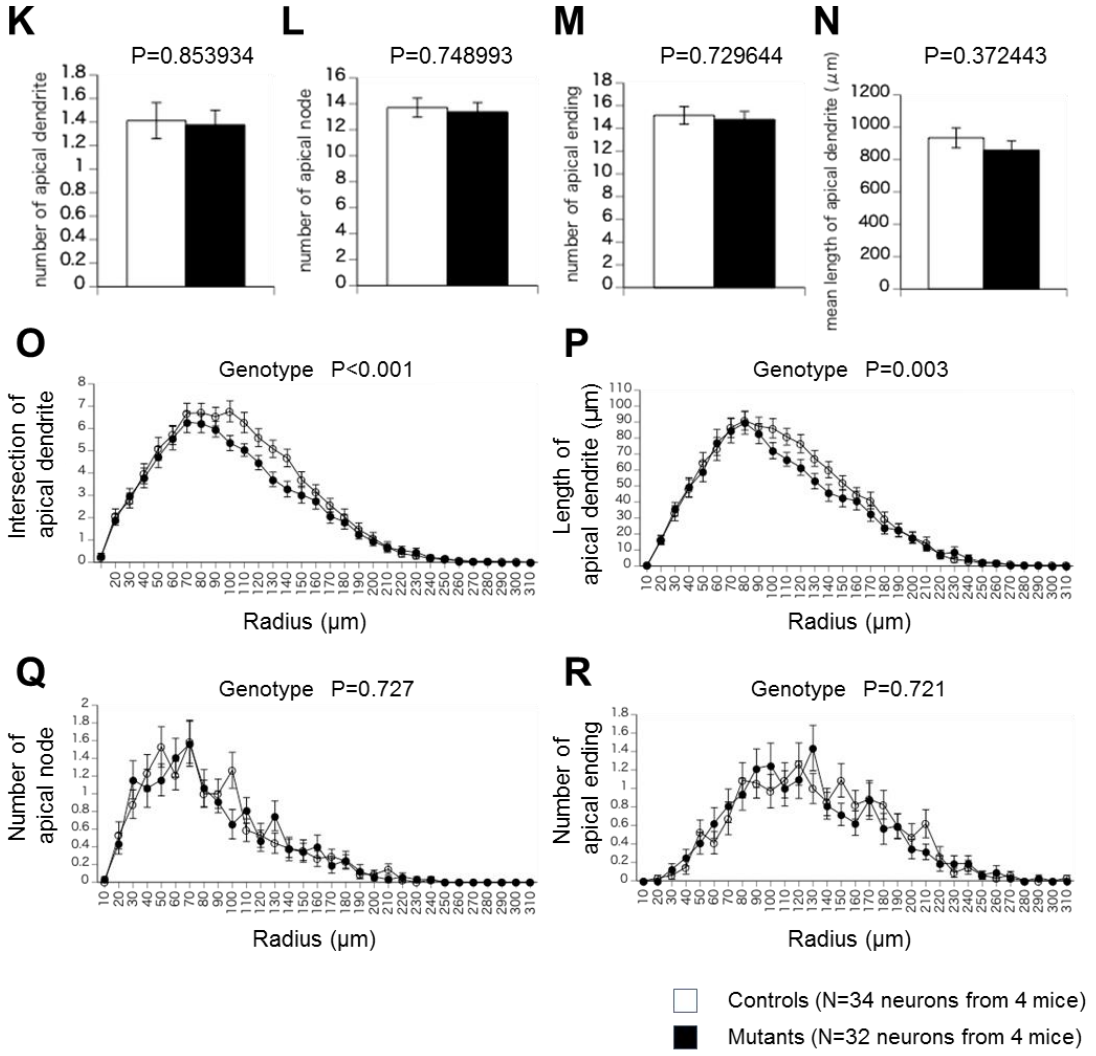

Figure 7. Abnormal dendritic arborization of the *Cdkl5* KO mouse demonstrated by Sholl analysis

A. Representative tracings using Neurolucida software.

B. Area of cell body (μm^2).

C – J. Arborization of basal dendrites. Total number of dendrites (C), nodes (D), endings (E) and mean length of dendrites (μm) (F) were measured.
Number of intersection (G), length of dendrites (H), number of nodes (I) and number of endings (J) in each 10 μm increment from the center of the soma were measured. The *Cdkl5* KO mice show less number and shorter length of basal dendrites.

K – R. Arborization of apical dendrites. Total number of dendrites (K), nodes (L),

endings (M) and mean length of dendrites (μm) (N) were measured.
Number of intersection (O), length of dendrites (P), number of nodes (Q) and number of endings (R) in each 10 μm increment from the center of the soma were measured. The *Cdkl5* KO mice show less number and shorter length of basal dendrites.

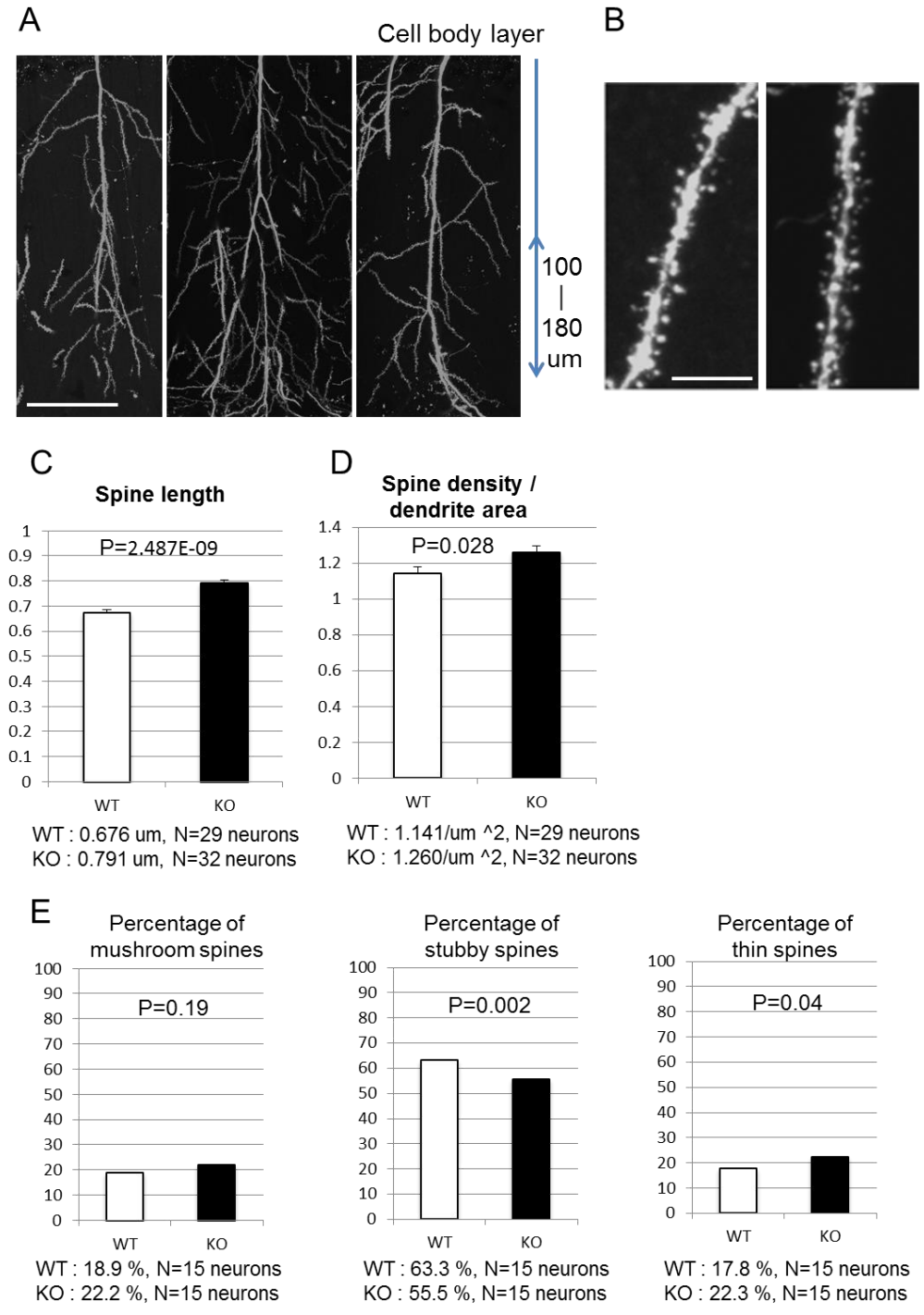

Fig. 8 Abnormal spine morphology and density in the *Cdkl5* KO mice.

A. Representative images of the CA1 apical dendrites of Thy1-EGFP positive *Cdkl5* KO mice. Scale bar = 50 um.

B. Magnified images. Scale bar = 5 um.

C. Spine length of the CA1 apical dendrites. The *Cdkl5* KO mice show significantly

increased spine length.

D. Spine density per dendritic surface area. The *Cdkl5* KO mice show significantly increased spine density.

E. Spine type classification. The bars show the percentage of mushroom spines (left), stubby spines (center) and thin spines (right). The *Cdkl5* KO mice show significantly decreased percentage of stubby spines (center) and increased percentage of thin spines (right).

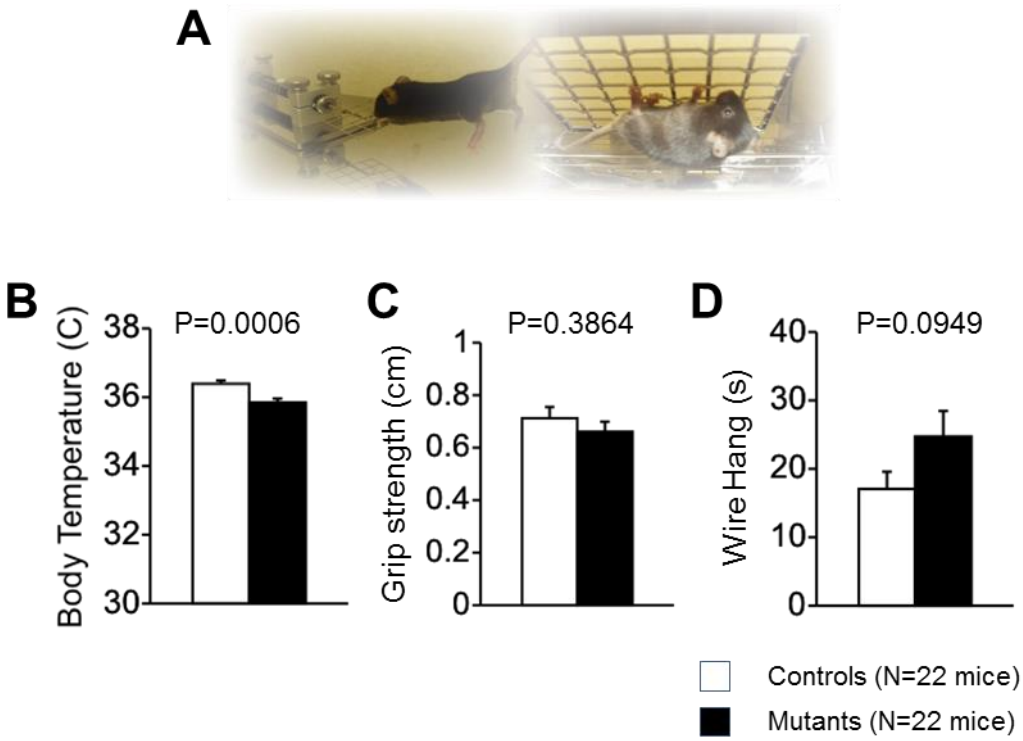

Figure 9. General health and motor functions of the *Cdkl5* KO mice

A. Images of grip strength (left) and wire hang test (right).

B. The *Cdkl5* KO mice show significantly lower body temperature (^{O}C) than wild type mice.

C. There is no significant difference in grip strength test (cm).

D. There is no significant difference in wire hang test (sec).

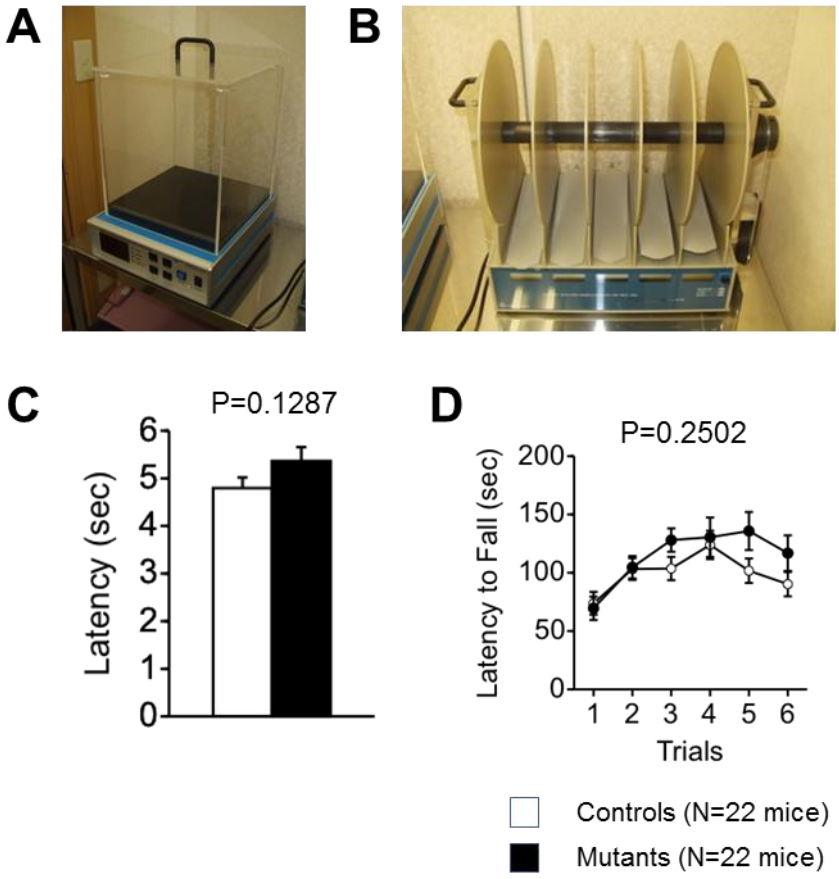

Figure 10. Hot plate test and rotarod test.

A. Hot plate test apparatus. B. Rotarod test apparatus.

C. There is no difference in latency to respond to the hot plate (sec).

D. There is no difference in latency to fall from the rotarod (sec).

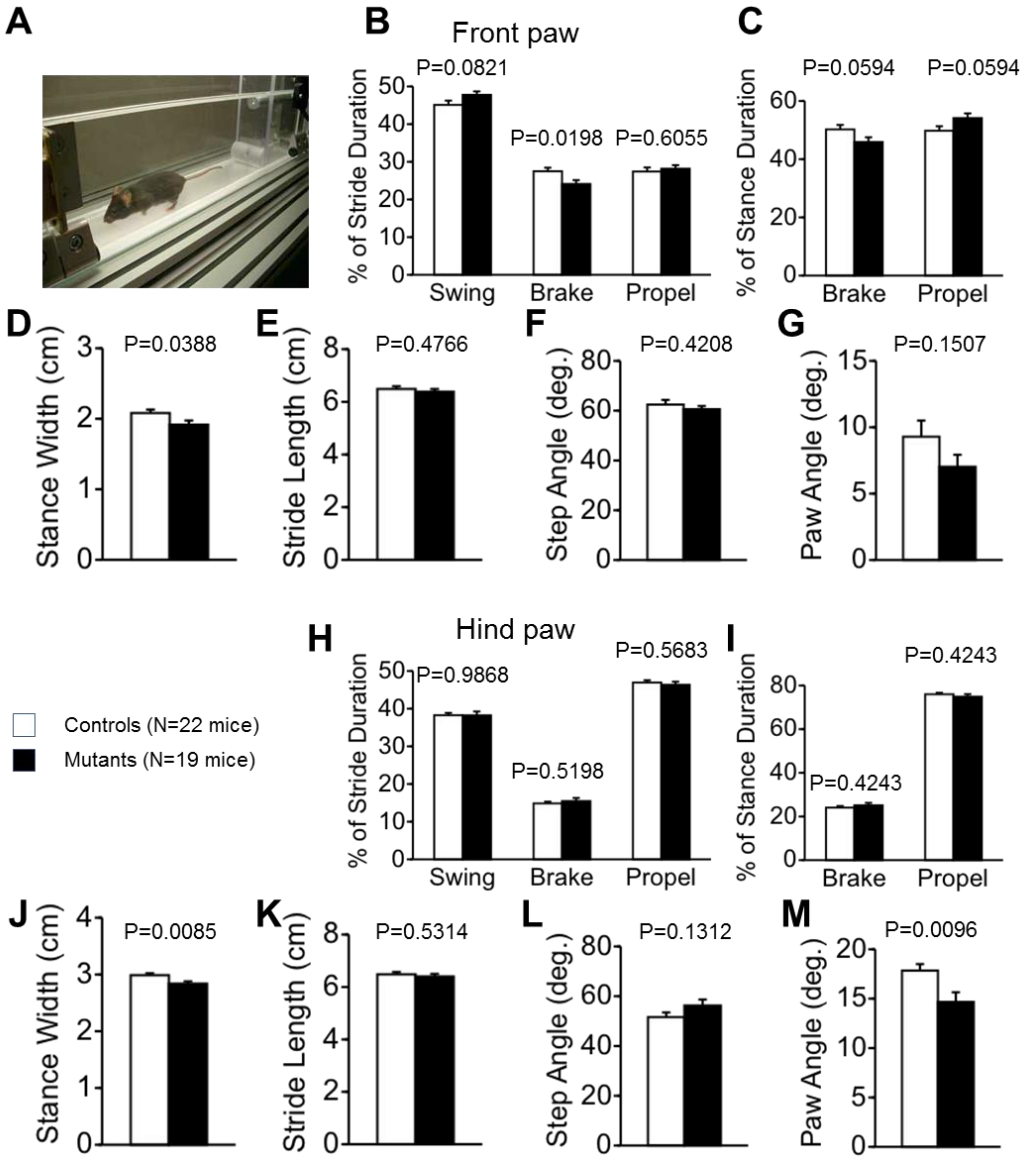

Figure 11. Gait analysis.

A. Image of the apparatus.

B – G. Gait analysis of front paws. The *Cdkl5* KO mice show significantly lower percentage of break duration (B) and decreased stance width (D). There are no differences in the percentage of stride duration (C), stride length (E), step angle (F) and paw angle (G).

H – M. Gait analysis of hind paws. The *Cdkl5* KO mice show significantly lower stance width (J) and lower paw angle (M). There are no differences in the percentage of stride duration (H), the percentage of stance duration (I), stride length (K) and step angle (L).

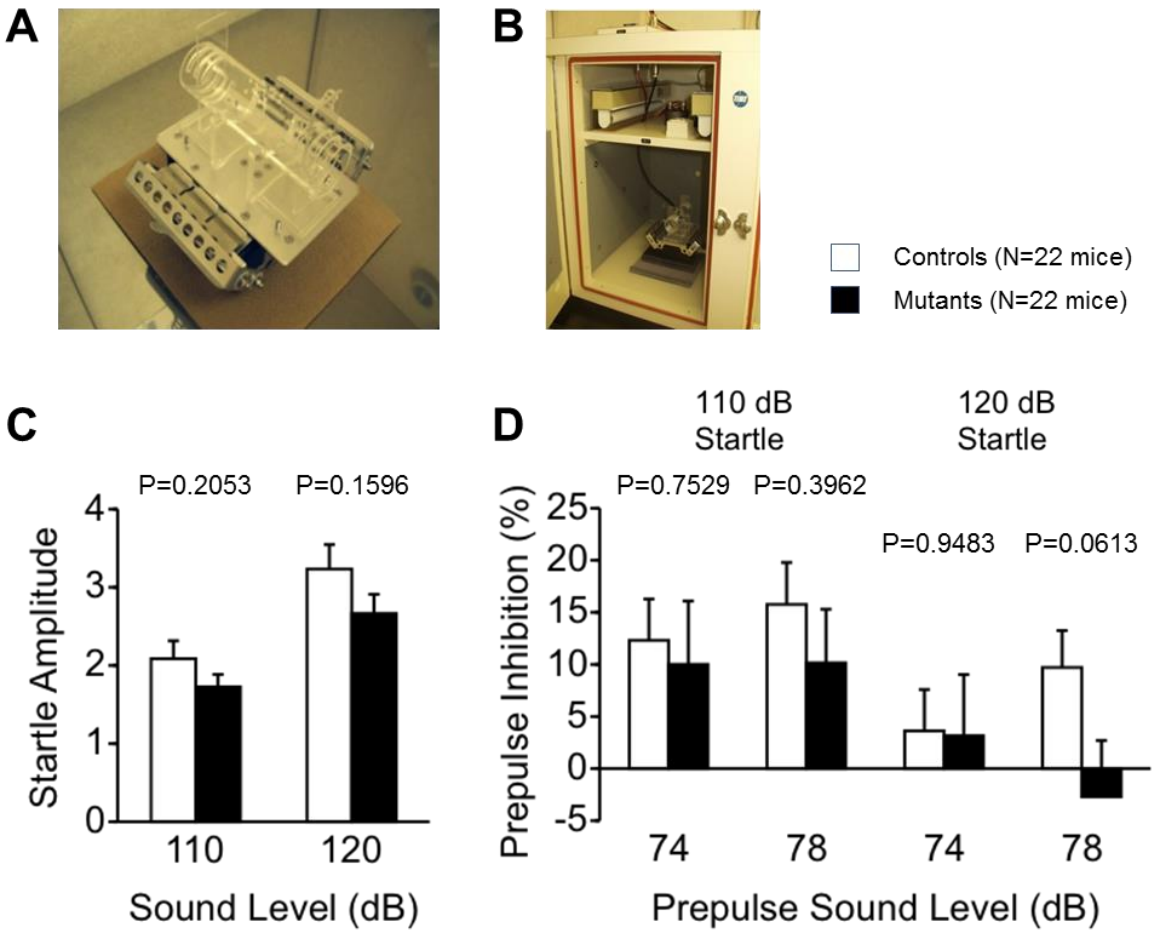

Figure 12. Startle response and prepulse inhibition tests

A. Plastic cylinder in which each mouse is placed (Takao and Miyakawa, 2009).

B. A soundproof chamber in which each plastic cylinder is placed (Takao and Miyakawa, 2009).

C. There is no difference in the startle response to 110 dB (left) and 120 dB (right).

D. There is no difference in the prepulse inhibition.

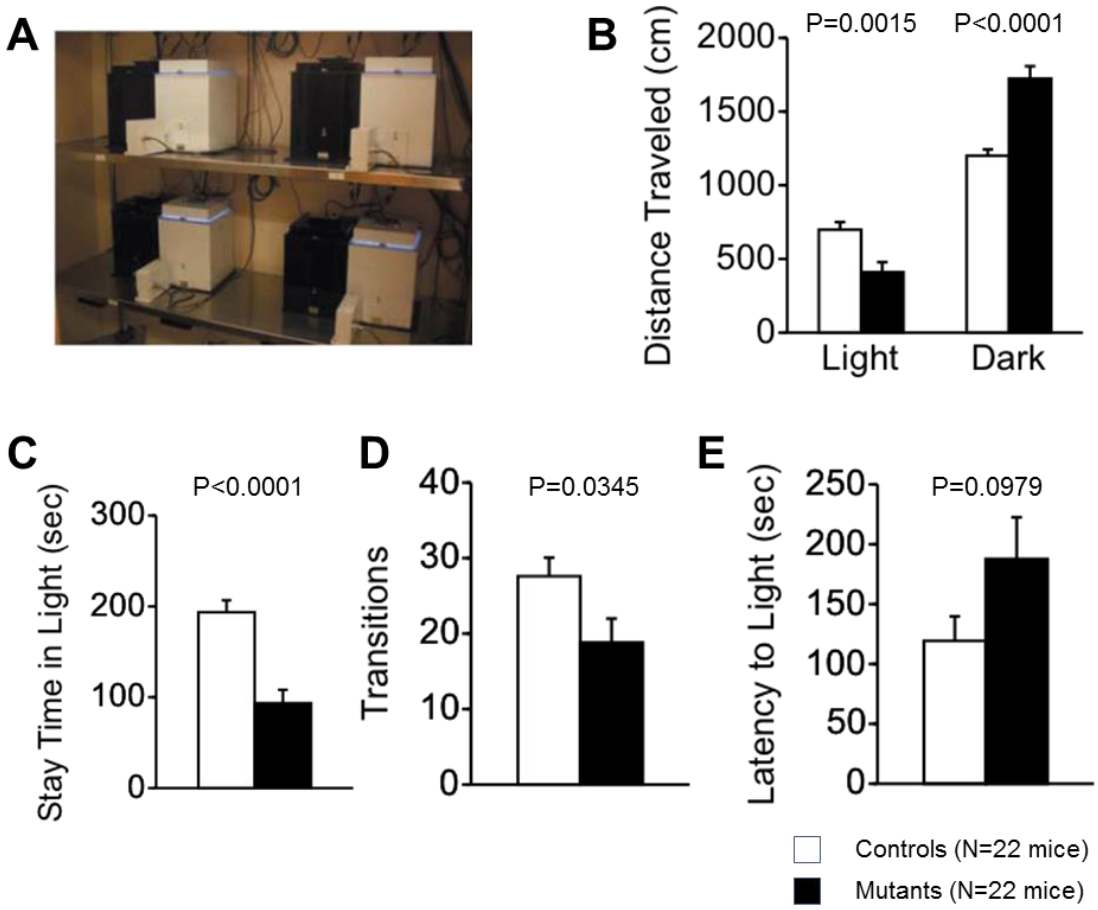

Figure 13. Light/dark transition test

A. Test apparatus (Takao and Miyakawa, 2009).

B. The *Cdkl5* KO mice show significantly decreased distance traveled in the light chamber (left) and increased distance traveled in the dark chamber (right).

C. The *Cdkl5* KO mice show significantly decreased stay time in the light chamber.

D. The *Cdkl5* KO mice also show significantly decreased number of transitions between chambers.

E. There is no significant difference in the latency to enter into the light chamber.

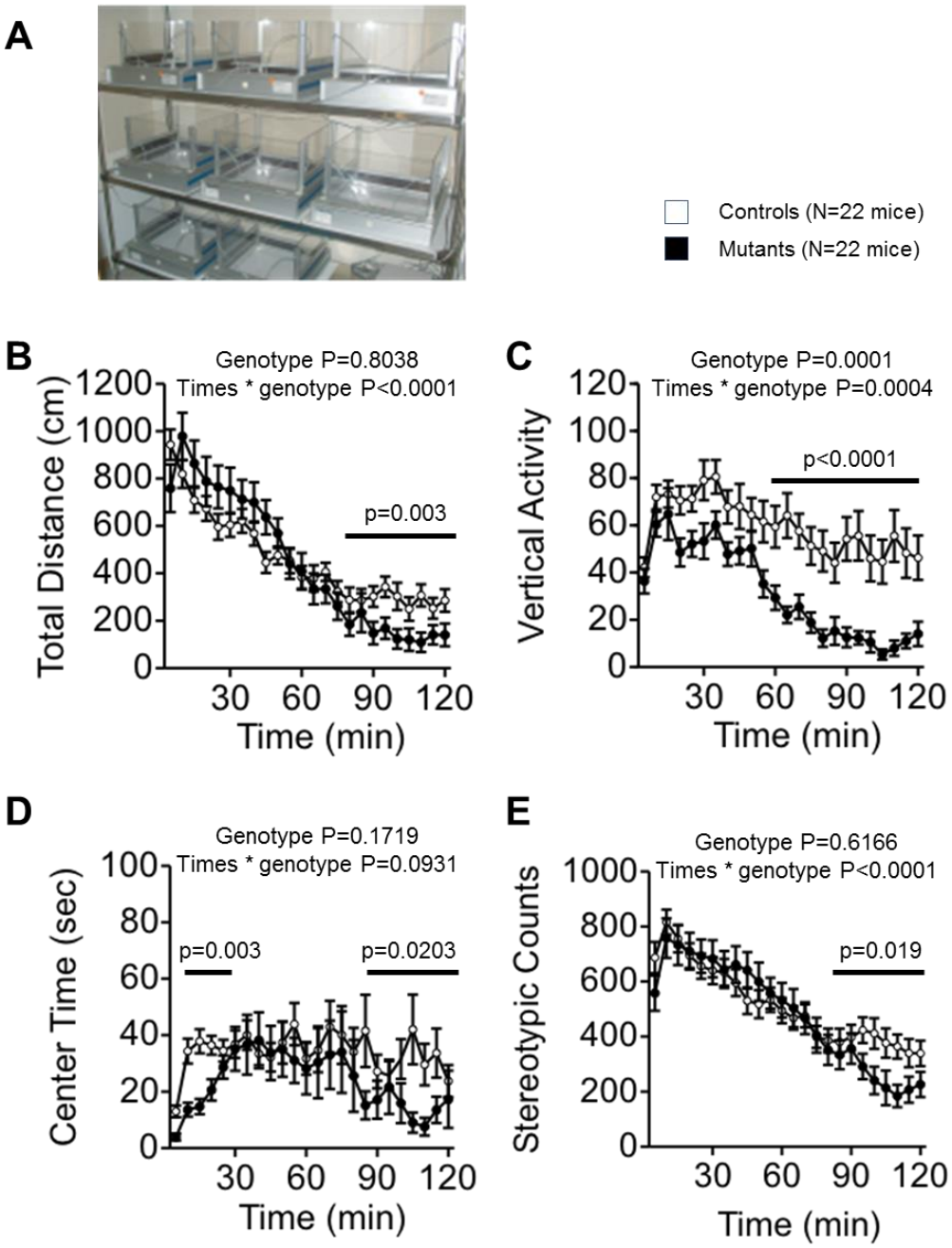

Figure 14. Open field test

A. Test apparatus. B. The *Cdkl5* KO mice show significantly decreased distance traveled during 90 – 120 minutes of test. C. The *Cdkl5* KO mice show significantly decreased number of vertical activity during 60 – 120 minutes of test. D. The *Cdkl5* KO mice show significantly decreased time spent in center during 0 – 30 and 90 – 120 minutes of test E. The *Cdkl5* KO mice show significantly decreased number of stereotypic behavior during 90 – 120 minutes of test.

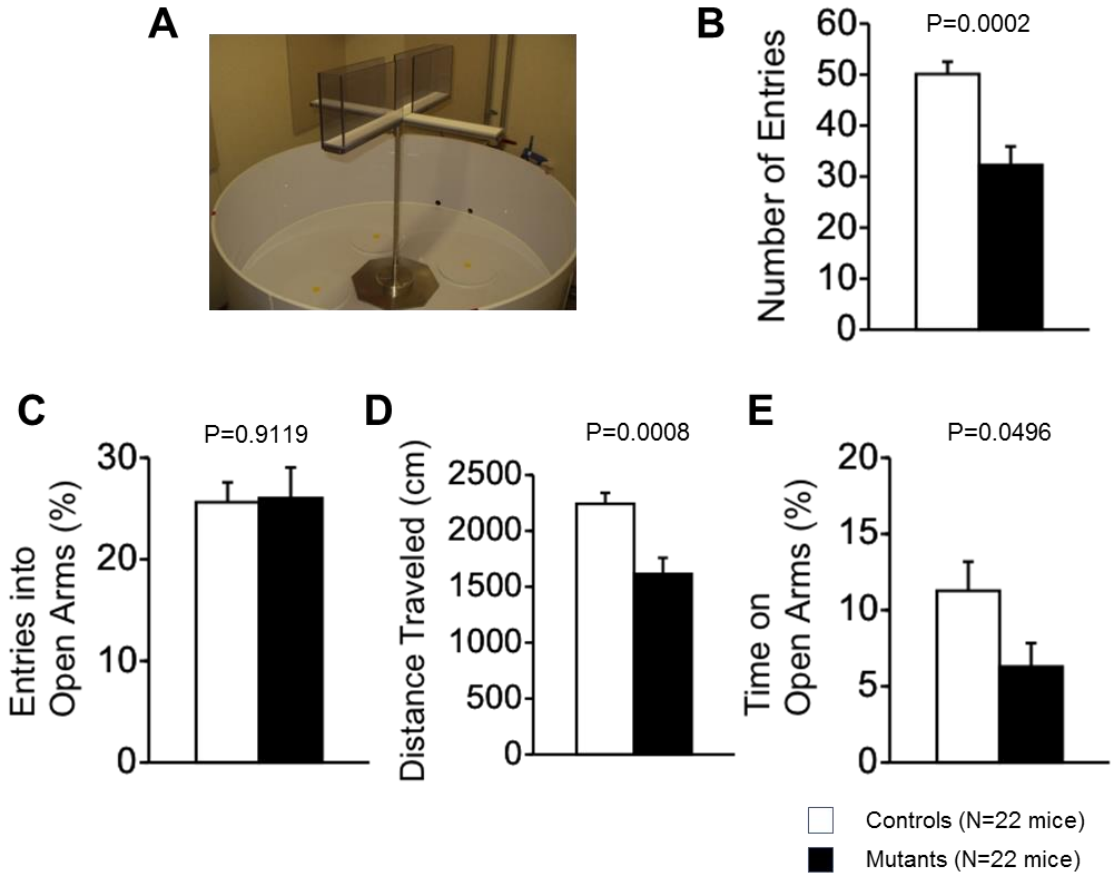

Figure 15. Elevated plus maze

A. Test apparatus (Takao and Miyakawa, 2009).

B. The *Cdkl5* KO mice show significantly decreased number of entries into all arms.

C. There is no significant difference in the percentage of the entries into open arms.

D. The *Cdkl5* KO mice show significantly decreased total distance traveled on the arms.

E. The *Cdkl5* KO mice show significantly decreased percentage of time spent on open arms.

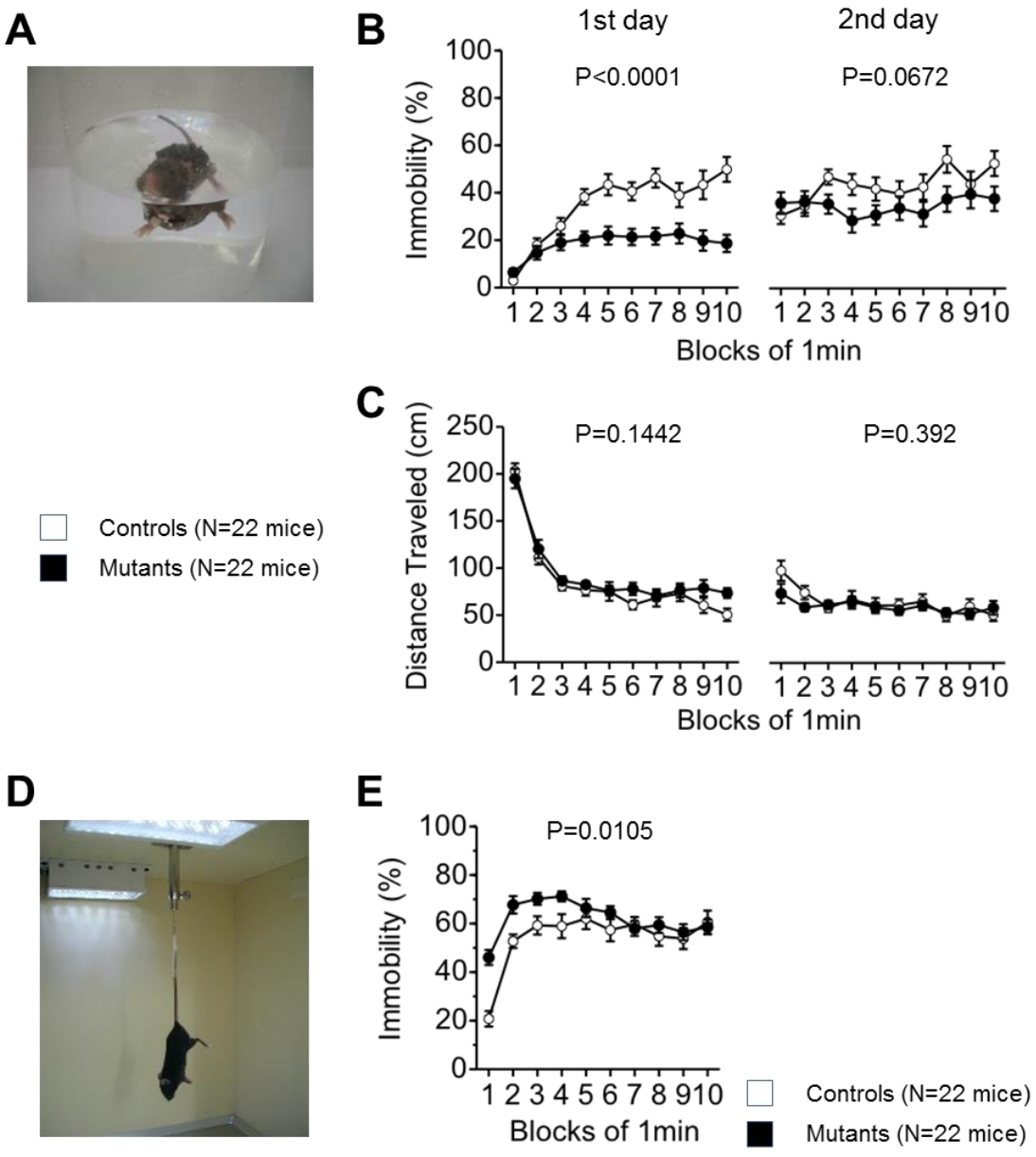

Figure 16. Porsolt forced swim test and tail suspension test

A. Image of Porsolt forced swim test.

B. The *Cdkl5* KO mice show decreased percentage of immobility in the 1st day (left), but not in the 2nd day (right). C. There is no significant difference in the distance traveled both in the 1st day (left) and the 2nd day (right).

D. Image of tail suspension test.

E. The *Cdkl5* KO mice show increased percentage of immobility.

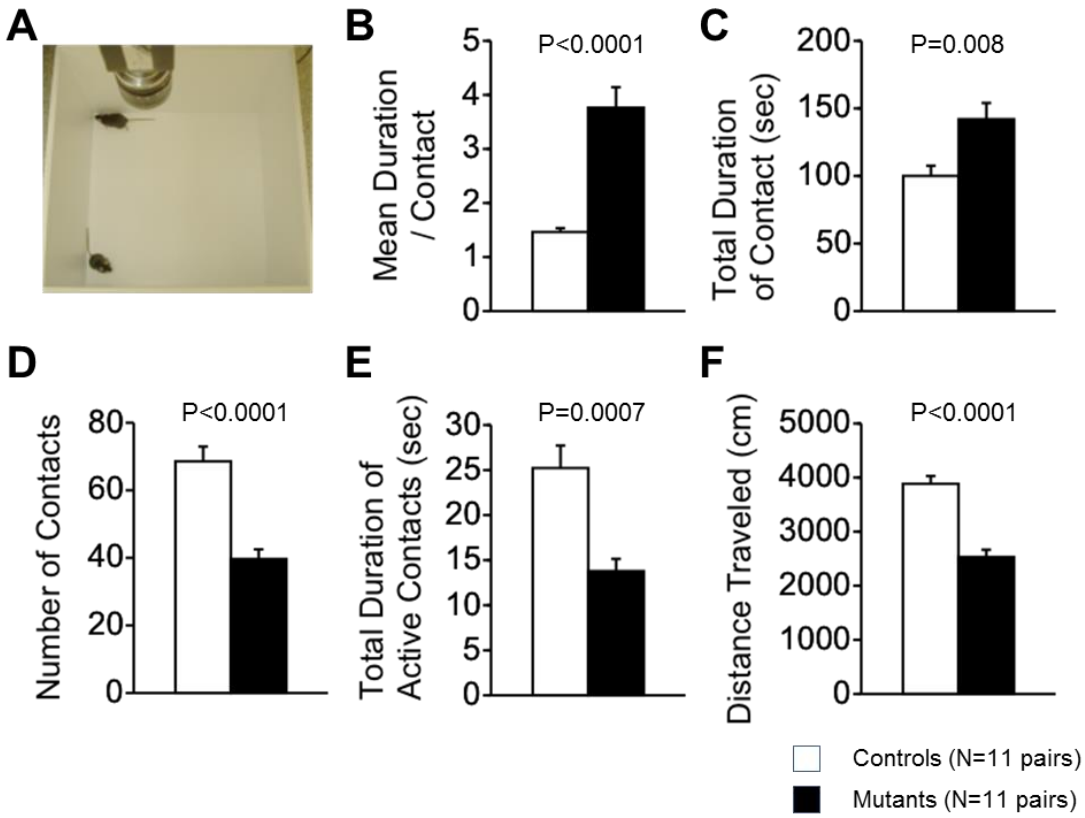

Figure 17. Social interaction test in novel environment (one chamber social interaction test)

A. Image of the test.

B. The *Cdkl5* KO mice show significantly increased mean duration per contact.

C. The *Cdkl5* KO mice show significantly increased total duration of contacts.

D. The *Cdkl5* KO mice show significantly decreased number of contacts.

E. The *Cdkl5* KO mice show significantly decreased total duration of active contacts.

F. The *Cdkl5* KO mice show significantly decreased distance traveled.

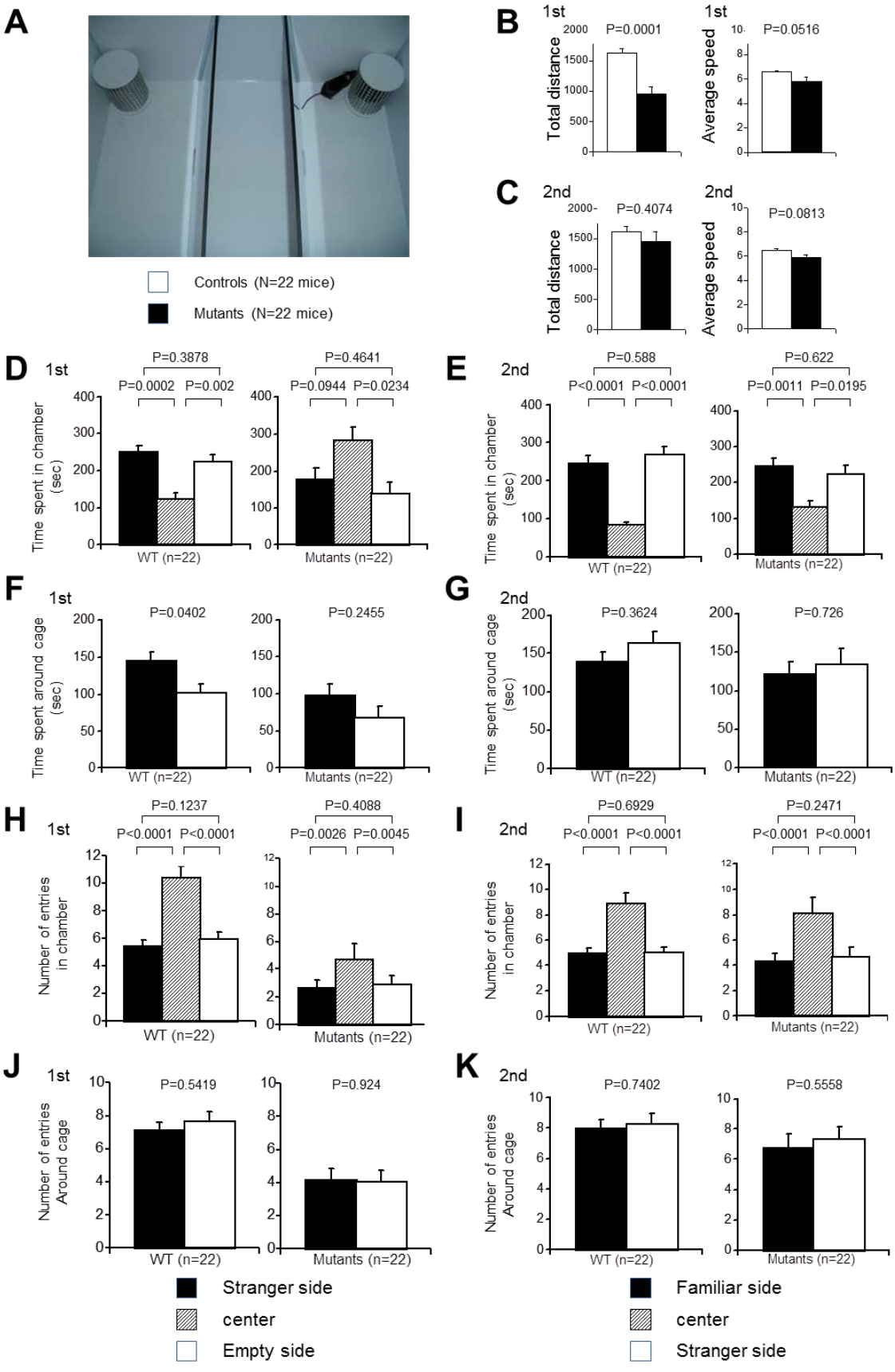
A
Controls (N=22 mice)
Mutants (N=22 mice)
B
1st
P=0.0001
Total distance
1st
P=0.0516
Average speed
C
2nd
P=0.4074
Total distance
2nd
P=0.0813
Average speed
D
1st
P=0.3878
P=0.0002
P=0.002
P=0.4641
P=0.0944
P=0.0234
Time spent in chamber (sec)
WT (n=22)
Mutants (n=22)
E
2nd
P=0.588
P<0.0001
P<0.0001
P=0.622
P=0.0011
P=0.0195
Time spent in chamber (sec)
WT (n=22)
Mutants (n=22)
F
1st
P=0.0402
P=0.2455
Time spent around cage (sec)
WT (n=22)
Mutants (n=22)
G
2nd
P=0.3624
P=0.726
Time spent around cage (sec)
WT (n=22)
Mutants (n=22)
H
1st
P=0.1237
P<0.0001
P<0.0001
P=0.4088
P=0.0026
P=0.0045
Number of entries in chamber
WT (n=22)
Mutants (n=22)
I
2nd
P=0.6929
P<0.0001
P<0.0001
P=0.2471
P<0.0001
P<0.0001
Number of entries in chamber
WT (n=22)
Mutants (n=22)
J
1st
P=0.5419
P=0.924
Number of entries Around cage
WT (n=22)
Mutants (n=22)
Stranger side
center
Empty side
K
2nd
P=0.7402
P=0.5558
Number of entries Around cage
WT (n=22)
Mutants (n=22)
Familiar side
center
Stranger side

Figure 18. Crawley's sociability and social novelty preference test (three chamber social interaction test)

A. Image of the test. The testing apparatus consists of a rectangular, three-chambered box and a lid. Each chamber is separated by walls made of clear Plexiglas, with small square openings (5 cm x 3 cm) allowing access into each chamber. Left and right chambers contain mouse cages.

B – C. The *Cdkl5* KO mice show significantly decreased total distance in the first session (B ; left), but no significant difference in the second session (C ; left). There are no significant differences in average speed in the first session (B ; right) and second session (C ; right).

D and E. Time spent in each chamber. In the first session, the wild type mice show significantly decreased time spent in the center chamber (D; left), but the *Cdkl5* KO mice show significantly increased time (D; right). In the second session, both the wild type mice and Cdkl5 KO mice show significantly decreased time spent in the center chamber (E).

F and G. Time spent around each cage. In the first session, the wild type mice show significantly increased time spent around the stranger mouse cage (F; left), but the *Cdkl5* KO mice show no significant difference (F; right). In the second session, both the wild type mice and *Cdkl5* KO mice show no significant difference in time spent around cages between the stranger and familiar mice (G).

H and I. Number of entries in chambers. In the first session, both the wild type mice and the *Cdkl5* KO mice show no significant difference in number of entries in chambers between the empty and stranger mice (H). In the second session, both the wild type mice and the *Cdkl5* KO mice also show no significant difference in number of entries in chambers between the stranger and familiar mice (I).

J and K. Number of entries around cage. In the first session, both the wild type mice and the *Cdkl5* KO mice show no significant difference in number of entries around cages between the empty and stranger mice (J). In the second session, both the wild type mice and the *Cdkl5* KO mice also show no significant difference in number of entries around cages between the stranger and familiar mice (K).

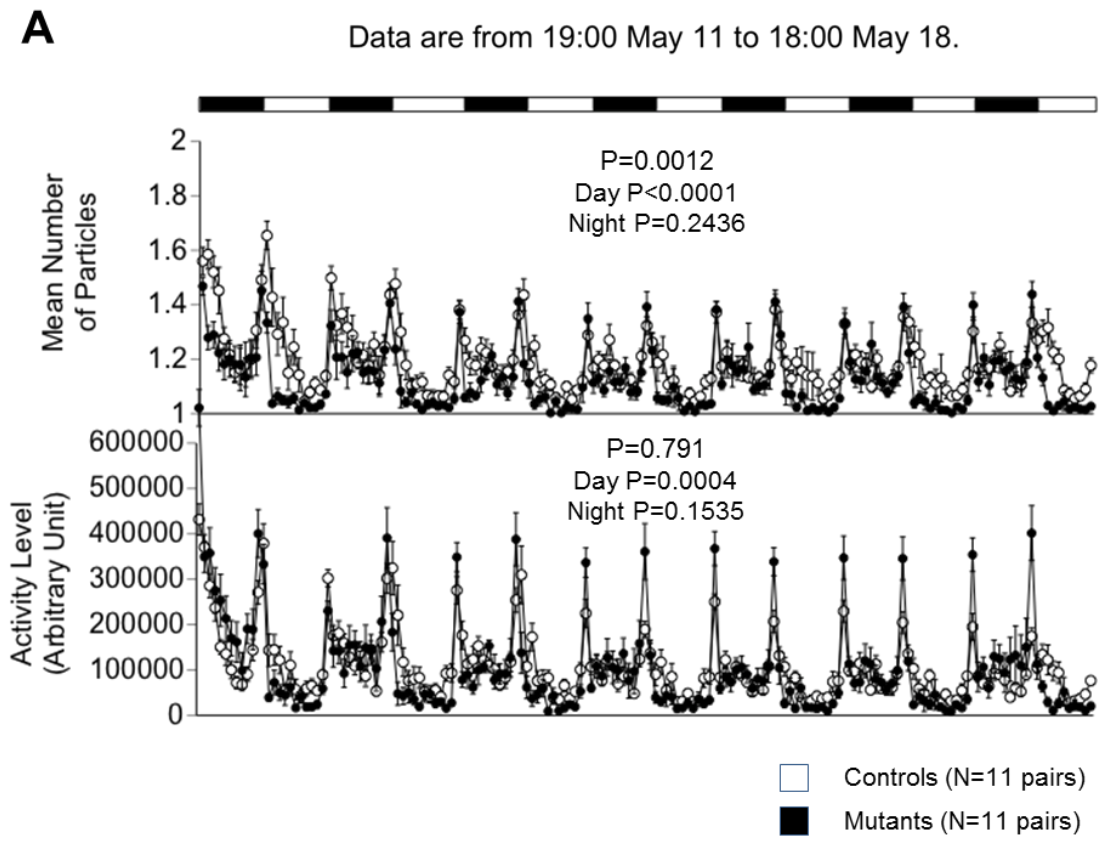

Figure 19. Twenty-four hour monitoring in the home cage

A. The *Cdkl5* KO mice show significantly decreased mean number of particles in the day time, but not in the night time (upper). Also, The *Cdkl5* KO mice show significantly decreased activity level in the daytime, but not in the night time (bottom). B. The averaged graph over 3 days of mean number of particles (upper) and activity level (bottom). The *Cdkl5* KO mice show significantly decreased mean number of particles and activity level in the day time.

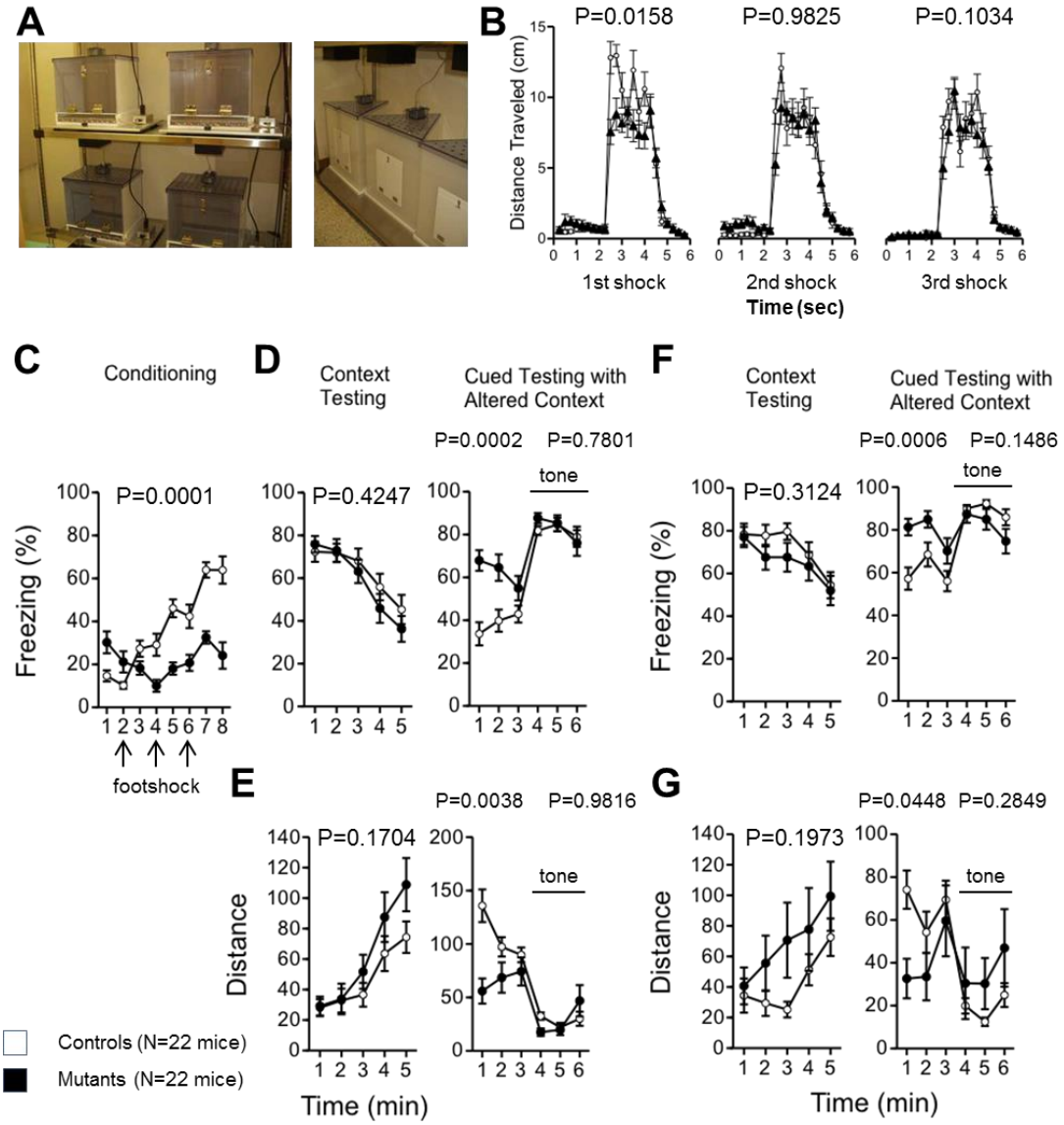

Figure 20. Contextual and cued fear conditioning test

A. Test apparatus. B. Distance traveled during time of 1st, 2nd, and 3rd shock.

C. The percentage of freezing during conditioning. The *Cdkl5* KO mice show significantly decreased percentage of freezing during conditioning.

D . One day after conditioning, the percentage of freezing during context testing (left) and cued testing with altered context (right).

E. One day after conditioning, distance traveled during context testing (left) and cued testing with altered context (right).

The *Cdkl5* KO mice show no difference in context test (D and E ; left). But, the *Cdkl5* KO mice show significantly increased freezing (D ; right) and decreased distance traveled (E ; right) in the cued test during pre-tone.

F. Seven days after conditioning, the percentage of freezing during context testing (left) and cued testing with altered context (right).
G. Seven days after conditioning, distance traveled during context testing (left) and cued testing with altered context (right).

The *Cdkl5* KO mice show no difference in context test (F and G; left). The *Cdkl5* KO mice show significantly increased freezing (F ; right) and decreased distance traveled (G ; right) in the cued test during pre-tone.

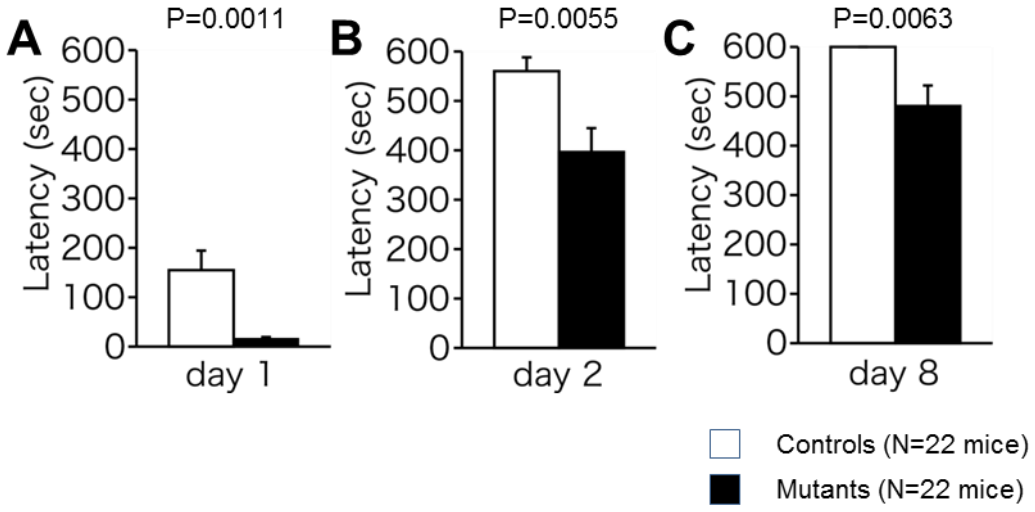

Figure 21. Passive avoidance test

Bar shows the latency to enter into the light chamber at day 1 (A), day 2 (B) and day 8 (C).

The *Cdkl5* mice show significantly decreased latency to enter into the light chamber at day 1 (A) , day 2 (B) and day 8 (C).

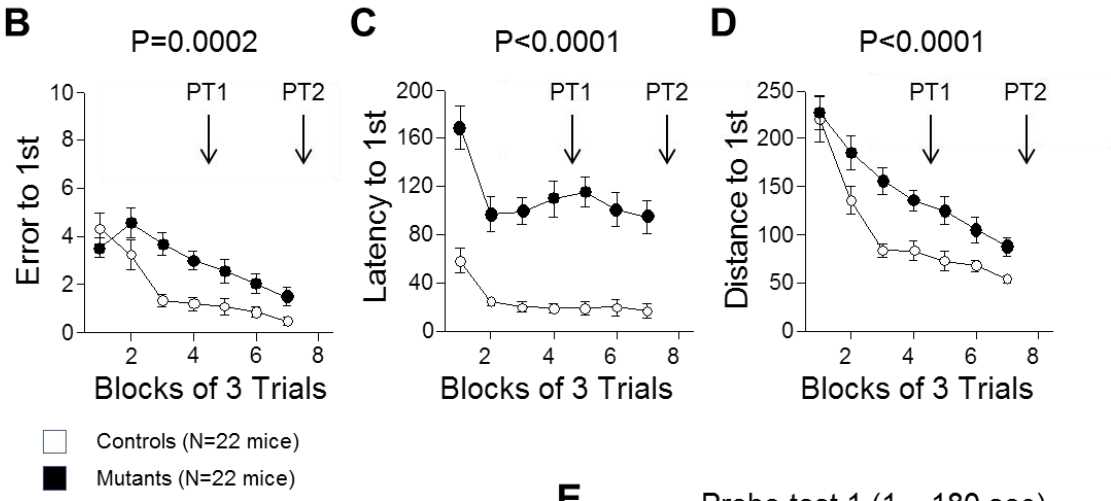
B
P=0.0002
PT1
PT2
Error to 1st
Blocks of 3 Trials
C
P<0.0001
PT1
PT2
Latency to 1st
Blocks of 3 Trials
D
P<0.0001
PT1
PT2
Distance to 1st
Blocks of 3 Trials
Controls (N=22 mice)
Mutants (N=22 mice)

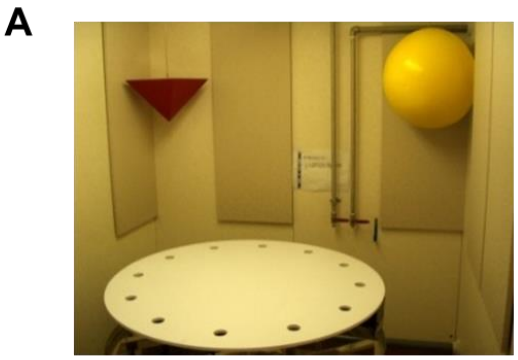
A

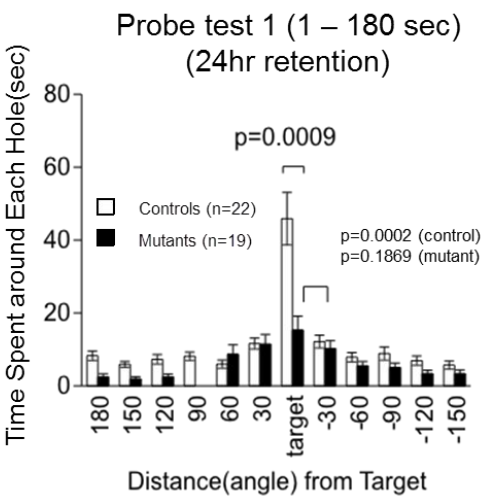
E
Probe test 1 (1 – 180 sec)
(24hr retention)
p=0.0009
Controls (n=22)
Mutants (n=19)
p=0.0002 (control)
p=0.1869 (mutant)
Time Spent around Each Hole(sec)
Distance(angle) from Target

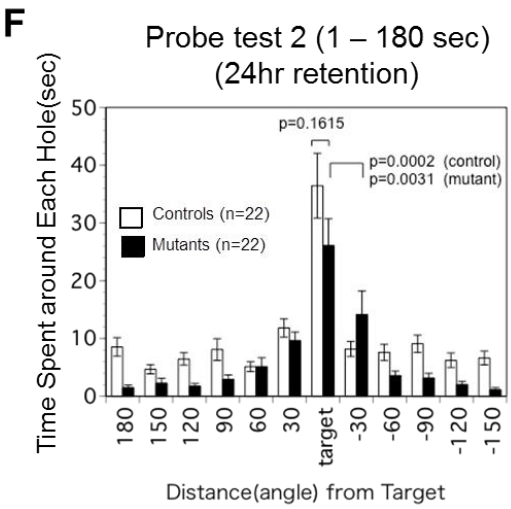
F
Probe test 2 (1 – 180 sec)
(24hr retention)
p=0.1615
p=0.0002 (control)
p=0.0031 (mutant)
Controls (n=22)
Mutants (n=22)
Time Spent around Each Hole(sec)
Distance(angle) from Target

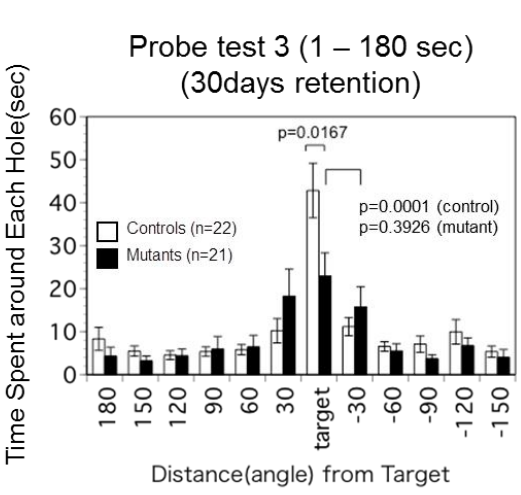
G
Probe test 3 (1 – 180 sec)
(30days retention)
p=0.0167
p=0.0001 (control)
p=0.3926 (mutant)
Controls (n=22)
Mutants (n=21)
Time Spent around Each Hole(sec)
Distance(angle) from Target

Figure 22. Barnes maze test

A. Test apparatus.

B – D. Number of errors before reaching the target (B), latency to reach the target (C) and distance traveled before reaching the target (D). PT1 and PT2 indicate probe test 1 and probe test 2, respectively. Data are presented as mean of 3 trials. The *Cdkl5* KO mice show significantly increased number of errors before reaching the target, latency to reach the target and distance traveled before reaching the target.

E – G. Time spent around each hole at the probe test 1 (E), the probe test 2 (after overtraining) (F) and the probe test 3 (after 30 day retention) (G).

In the probe test 1, the *Cdkl5* KO mice spent significantly less time around the target hole (E). After overtraining, the *Cdkl5* KO mice spent around the target hole to the similar extent of WT mice in the probe test 2 (F). But, after 30days retention, *Cdkl5* KO mice spent significantly less time around the target hole in the probe test 3 (G).

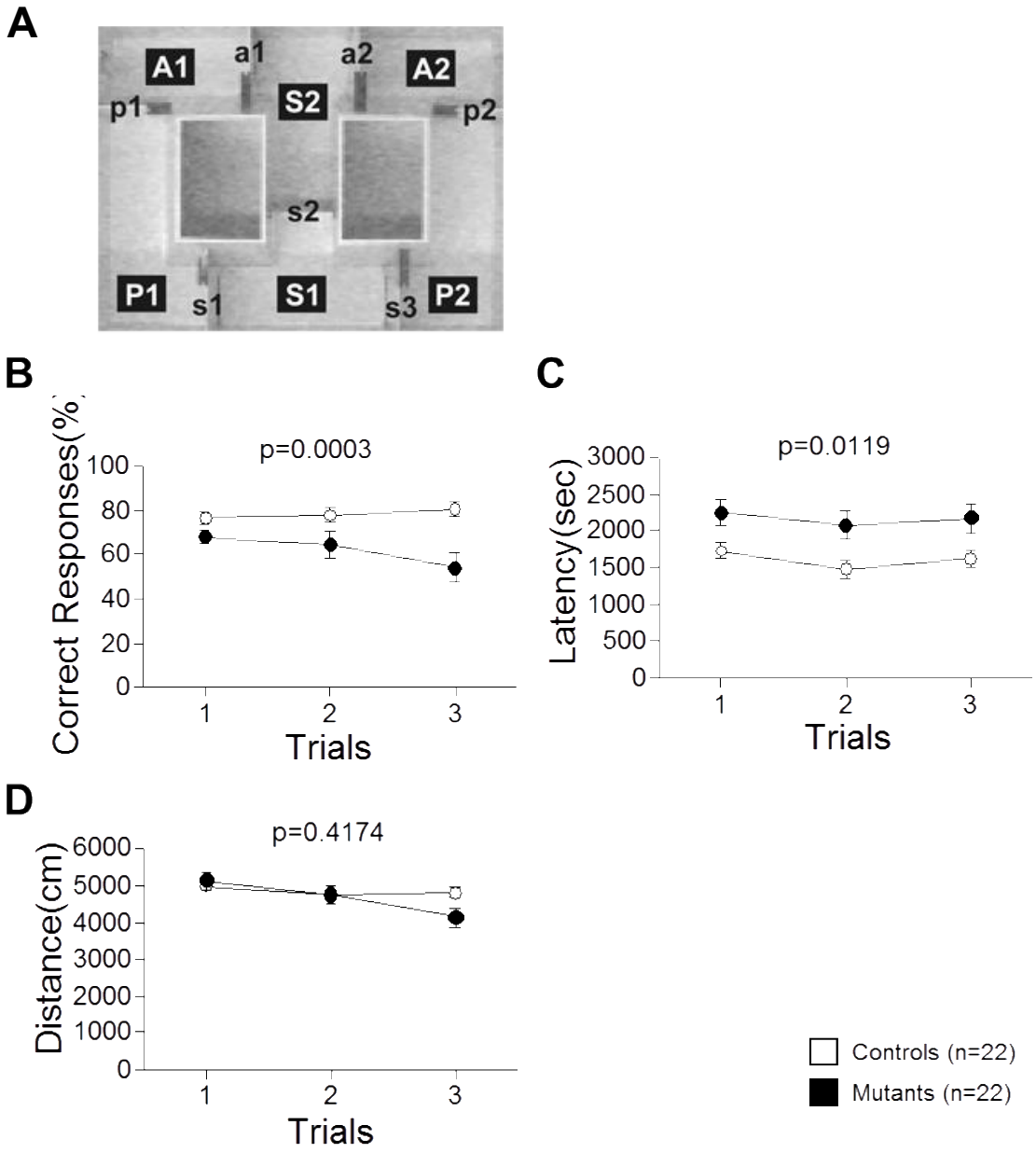

Figure 23. T-maze test

A. Image of the test.

B – D. *Cdkl5* KO mice show significantly decreased percentage of correct responses (B) and latency to finish trials (C) on trial 1, 2, and 3. But, there is no significant difference in the distance traveled (D).

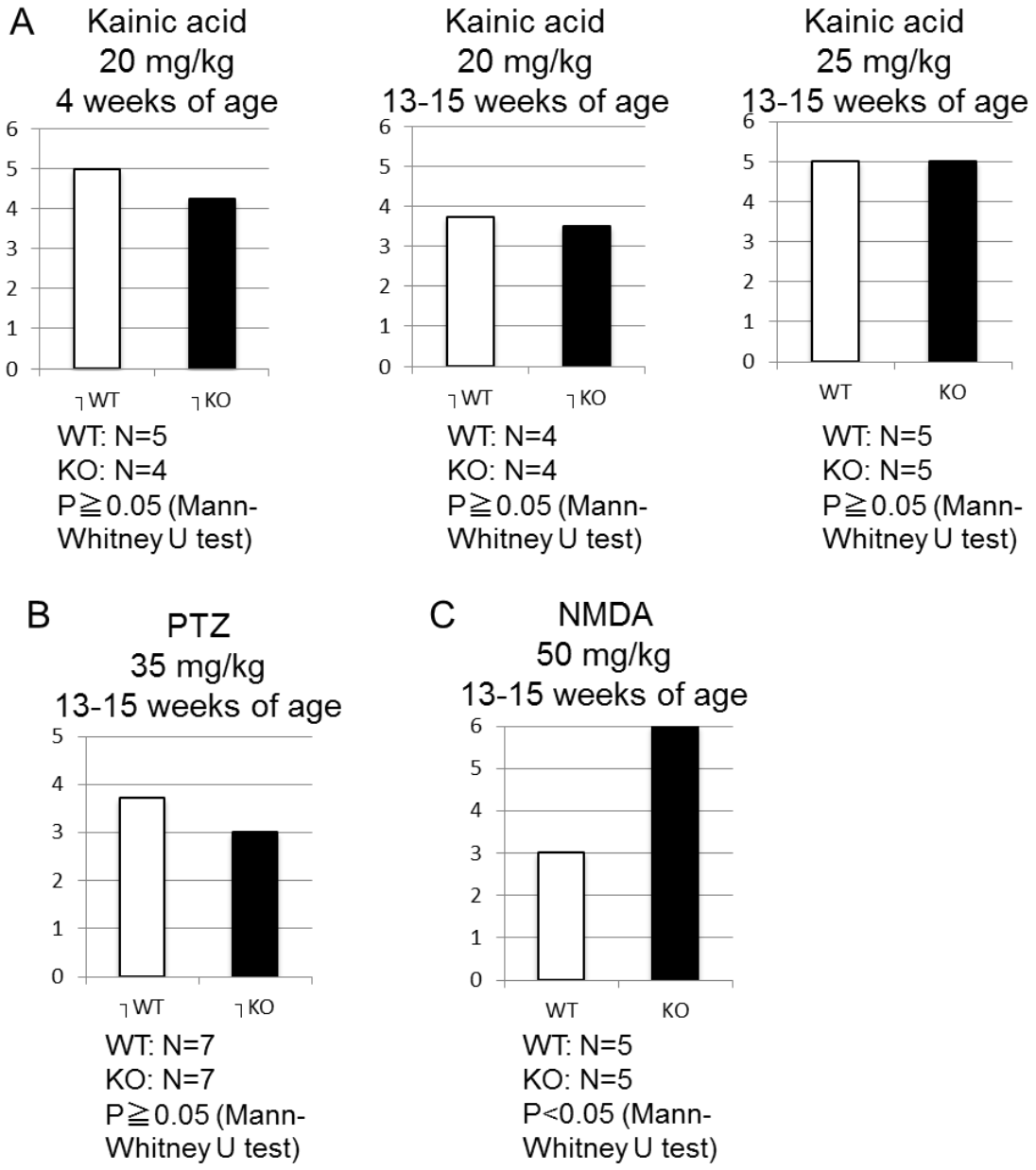

Figure 24. Enhanced seizure susceptibility of the *Cdkl5* KO mice in response to NMDA

A. Averaged max seizure scores induced by kainic acid. There are no differences in the seizure susceptibility in response to 20 mg/kg kainic acid between the wild type mice and the *Cdkl5* KO mice both in 4 weeks (left) and 13-15 weeks (center) of age. There is no difference in the seizure susceptibility in response to 25 mg/kg kainic acid (right).

B. Averaged max seizure scores induced by PTZ. There is no difference in the seizure susceptibility in response to 35 mg/kg PTZ between the wild type mice and the *Cdkl5* KO mice.

C. Averaged max seizure scores induced by NMDA. The *Cdkl5* KO mice show significantly increased seizure susceptibility in response to 50 mg/kg NMDA.

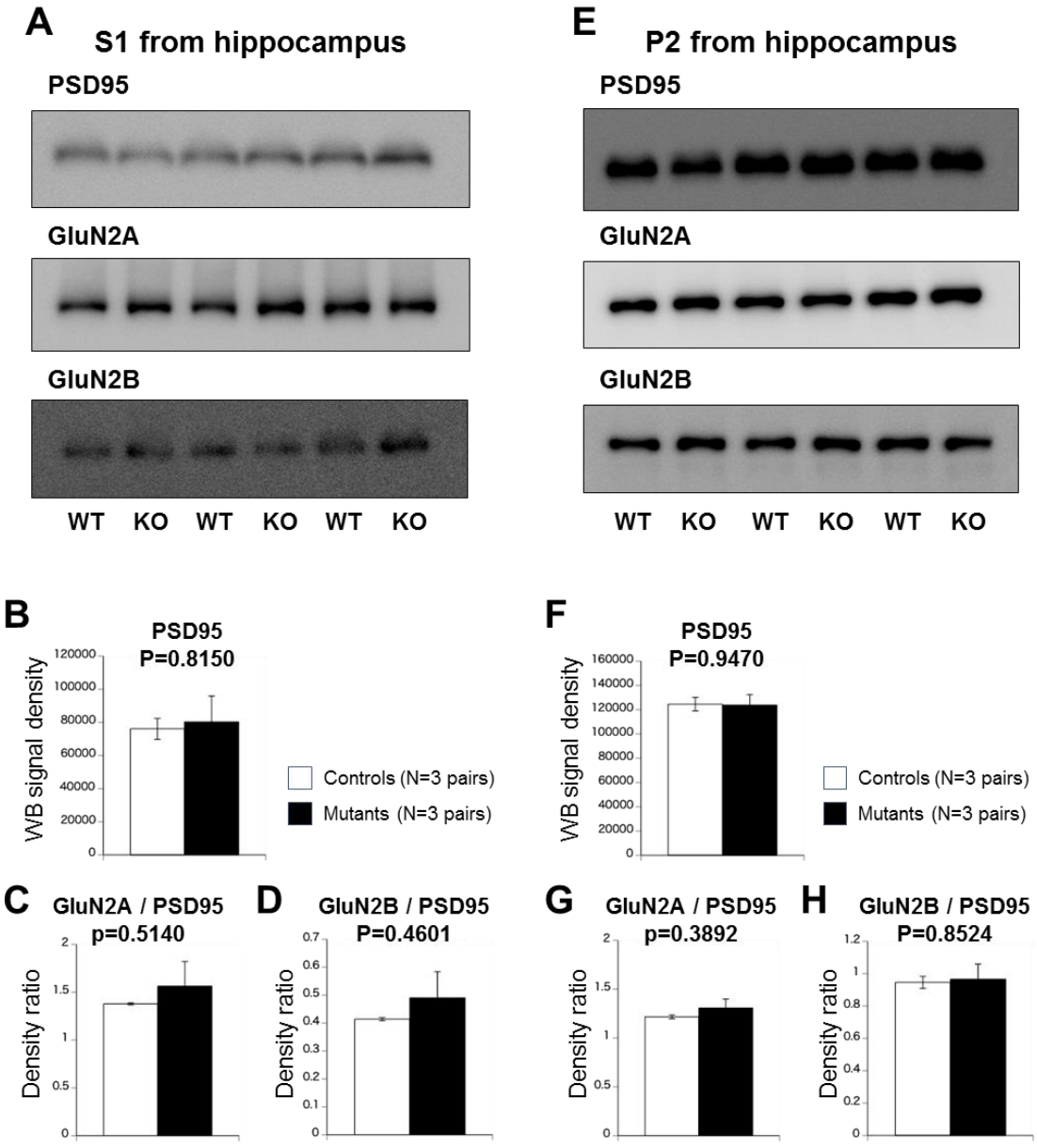

Figure 25. GluN2B subunit is aberrantly accumulated at the postsynapses of the *Cdkl5* KO mice

A. Images of western blotting of S1 fraction from hippocampi.

B – D. There are no differences in signal intensity of PSD-95 per loading protein (B), GluN2A normalized by PSD-95 (C) and GluN2B normalized by PSD-95 (D) between the wild type mice and the *Cdkl5* KO mice.

E. Images of western blotting of P2 fraction from hippocampi.

F – H. There are no differences in signal intensity of PSD-95 per loading protein (F), GluN2A normalized by PSD-95 (G) and GluN2B normalized by PSD-95 (H) between the wild type mice and the *Cdkl5* KO mice..

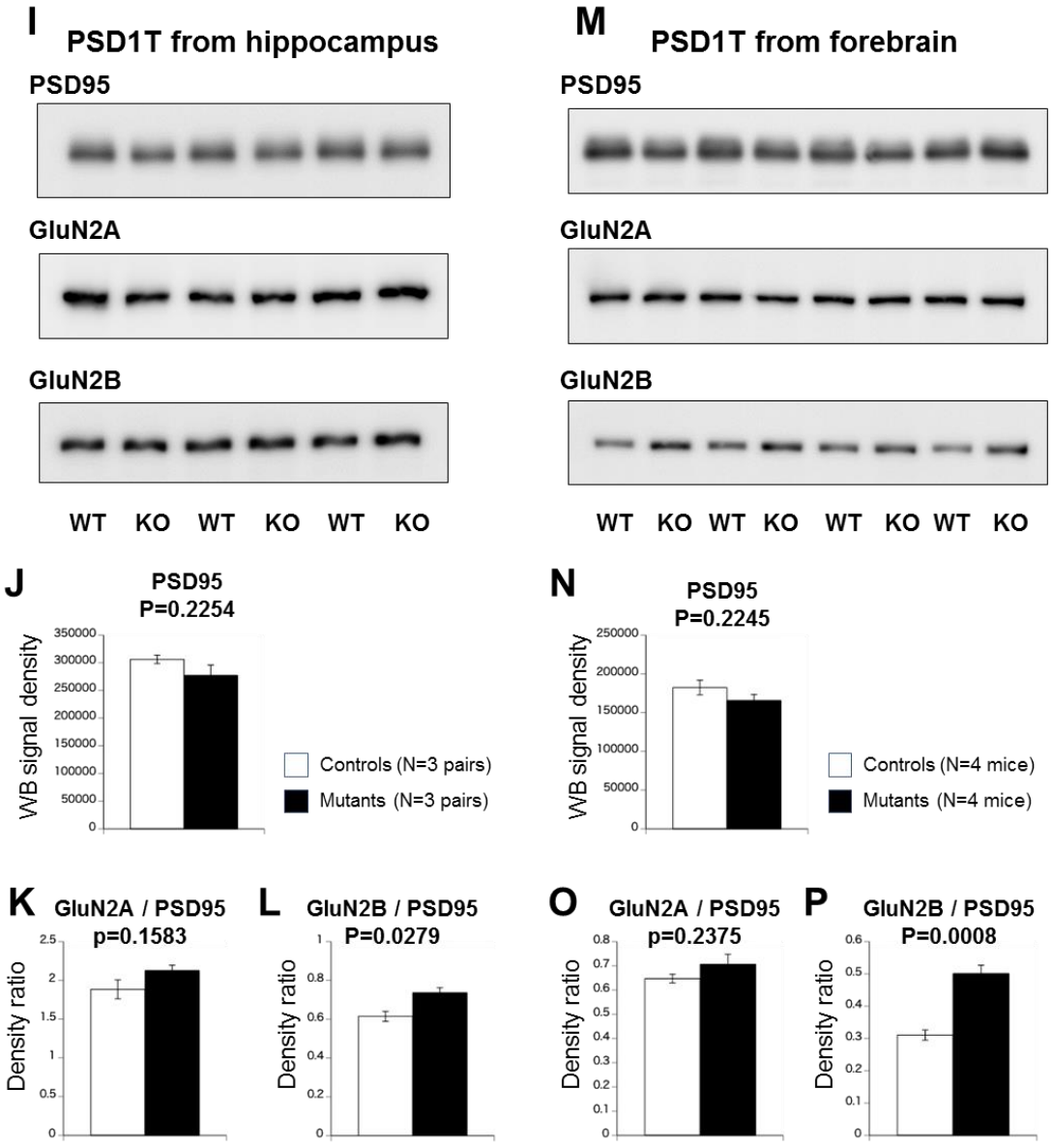

Figure 25 (continued). GluN2B subunit is aberrantly accumulated at the postsynapses of the *Cdkl5* KO mice

I. Images of western blotting of PSD-1T fraction from hippocampi.

J – L. There are no differences in signal intensity of PSD-95 per loading protein (J) and GluN2A normalized by PSD-95 (K) between the wild type mice and the *Cdkl5* KO mice, but the *Cdkl5* KO mice show significantly increased signal intensity of GluN2B normalized by PSD-95 (L).

M. Images of western blotting of PSD-1T fraction from forebrain.

N – P. There are no differences in signal intensity of PSD-95 per loading protein (N) and GluN2A normalized by PSD-95 (O) between the wild type mice and the *Cdkl5* KO

mice, but the *Cdkl5* KO mice show significantly increased signal intensity of GluN2B normalized by PSD-95 (P).

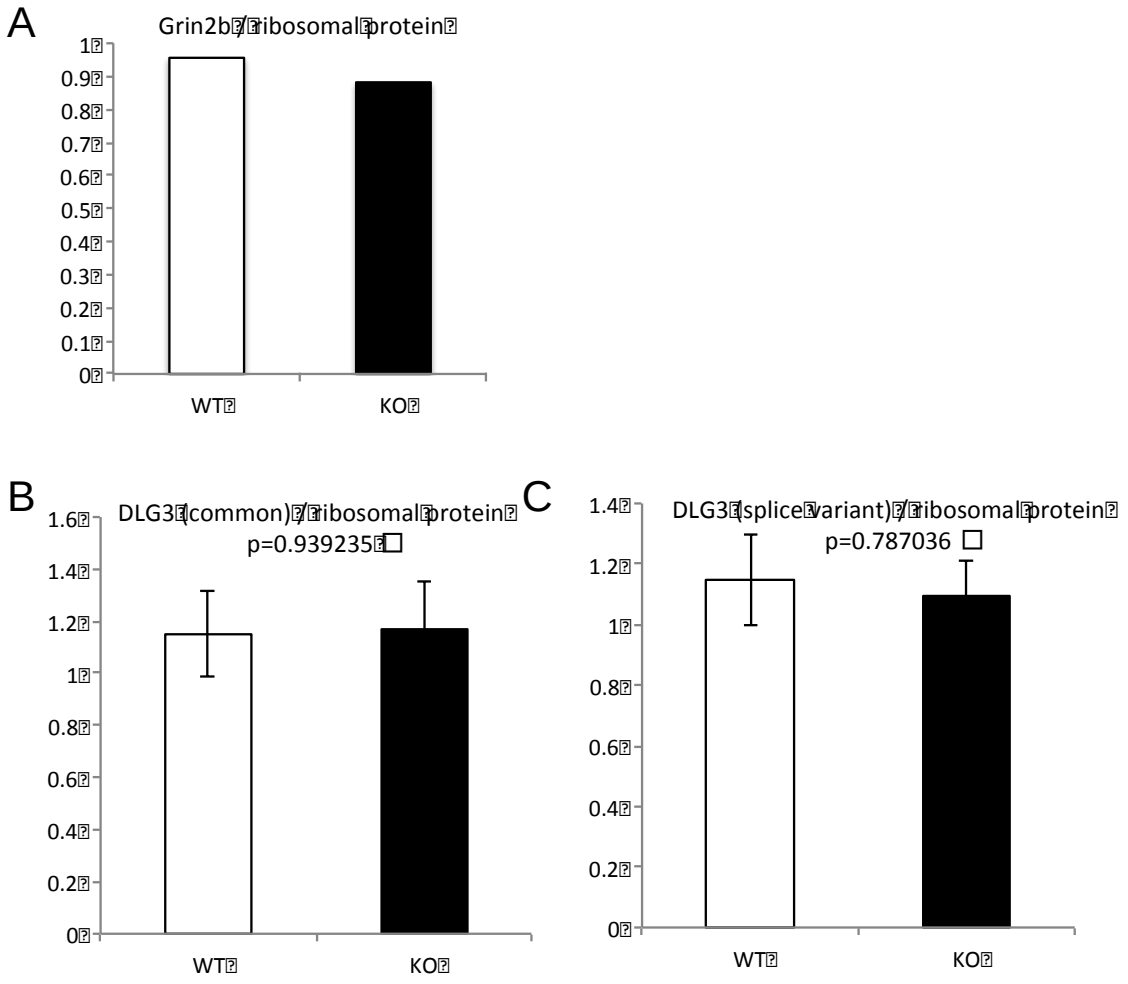

Figure 26. No change in Grin2b and Dlg3 mRNA level in the *Cdkl5* KO mice

A – C. There are no differences in mRNA ratio of Grin2b / Ribosomal protein S18 (A), Dlg3 / Ribosomal protein S18 (B) and Dlg3 (splice variant) / Ribosomal protein S18 (C).

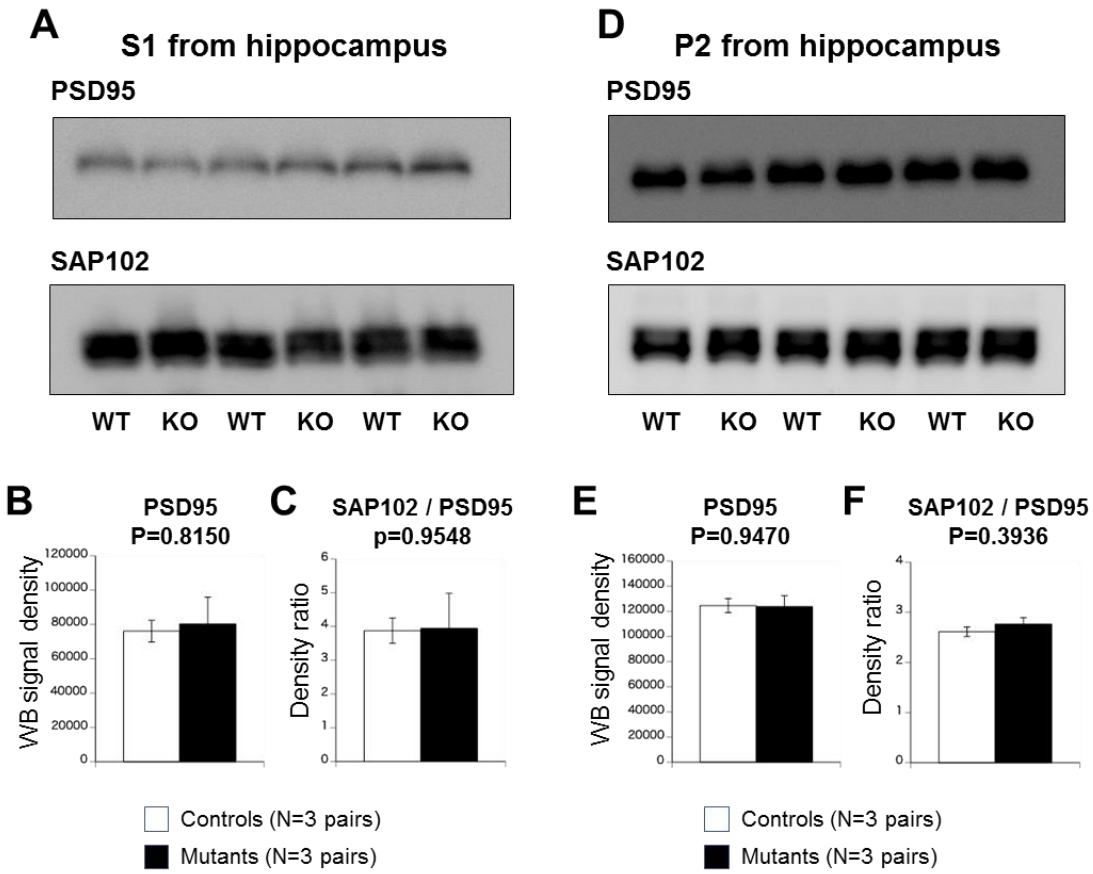

Figure 27. SAP102 is accumulated at postsynapses of the *Cdkl5* KO mice

A. Images of western blotting of S1 fraction from hippocampi.

B and C. There are no differences in signal intensity of PSD-95 per loading protein (B) and SAP102 normalized by PSD-95 (C) between the wild type mice and the *Cdkl5* KO mice.

D. Images of western blotting of P2 fraction from hippocampi.

E and F. There are no differences in signal intensity of PSD-95 per loading protein (E) and SAP102 normalized by PSD-95 (F) between the wild type mice and the *Cdkl5* KO mice.

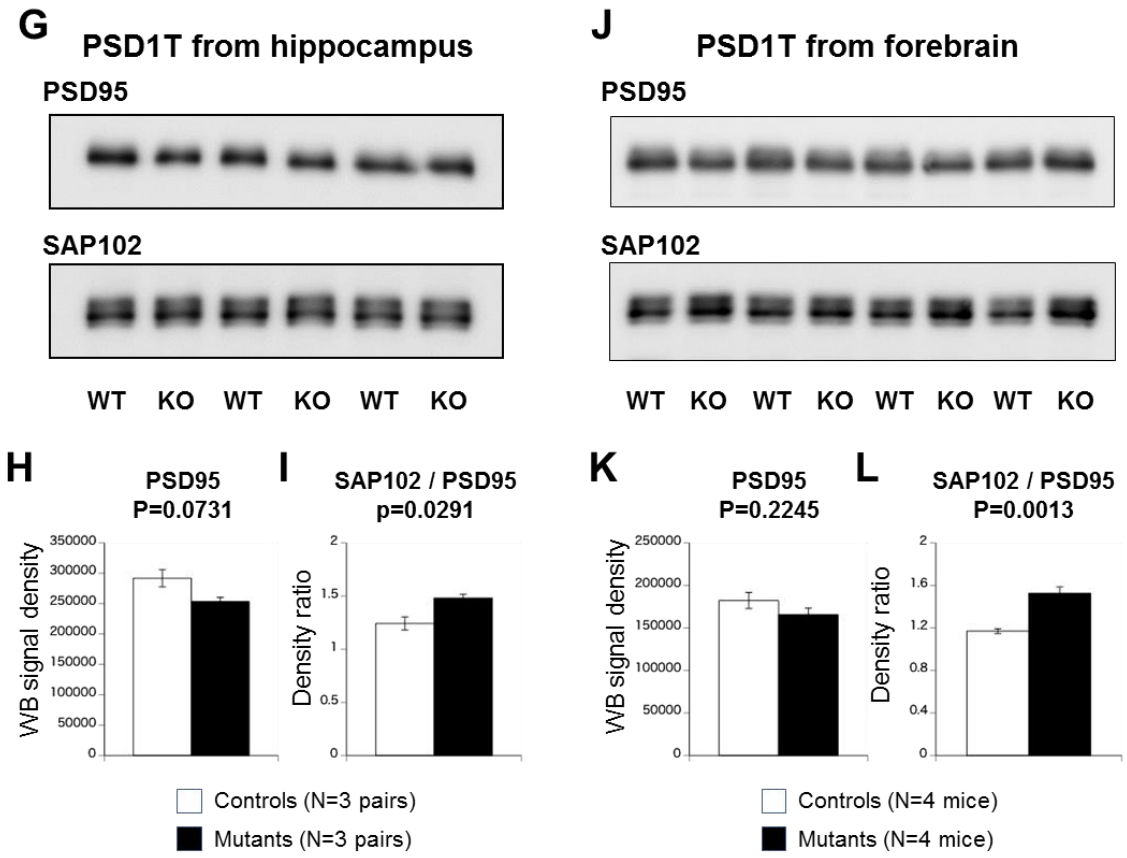

Figure 27 (continued). SAP102 is accumulated at postsynapses of the *Cdkl5* KO mice

G. Images of western blotting of PSD-1T fraction from hippocampi.

H and I. There is no difference in signal intensity of PSD-95 per loading protein (H), but the *Cdkl5* KO mice show significantly increased signal intensity of SAP102 normalized by PSD-95 (I).

J. Images of western blotting of PSD-1T fraction from forebrain.

K and L. There is no difference in signal intensity of PSD-95 per loading protein (K), but the *Cdkl5* KO mice show significantly increased signal intensity of SAP102 normalized by PSD-95 (L).